

# Mineralogy, geochemistry, and genesis of lateritic bauxite deposits in the Wuchuan–Zheng'an–Daozhen area, Northern Guizhou Province, China

Jing Gu <sup>a,b</sup>, Zhilong Huang <sup>a,\*</sup>, Hongpeng Fan <sup>a</sup>, Zhongguo Jin <sup>c</sup>, Zaifei Yan <sup>a</sup>, Jiawei Zhang <sup>a</sup>

<sup>a</sup> State Key Laboratory of Ore Deposit Geochemistry, Institute of Geochemistry, Chinese Academy of Sciences, 46 Guanshui Road, Guiyang 550002, China

<sup>b</sup> Graduate University of Chinese Academy of Sciences, Beijing 100049, China

<sup>c</sup> Guizhou Nonferrous Metal and Nuclear Industry Geological Exploration Bureau, Guiyang 550005, China

## ARTICLE INFO

### Article history:

Received 18 July 2012

Accepted 18 March 2013

Available online 26 March 2013

### Keywords:

Lateritic bauxite deposit

Mineralogy

Geochemistry

Wuchuan–Zheng'an–Daozhen area

Precursor

Ore-forming process

## ABSTRACT

The lateritic bauxite deposits in the Wuchuan–Zheng'an–Daozhen area, Northern Guizhou Province, are hosted by the Liangshan Formation which unconformably overlies the Lower–Middle Silurian mud-shale and the Upper Carboniferous limestone and underlies the Middle Permian limestone. From the bottom upward, the deposits are generally composed of brick-red, yellow-brown, and gray bauxite horizons. Diaspore, boehmite, kaolinite, smectite and hematite are the major mineral components in the bauxite ores with small amounts of gibbsite, illite, goethite, pyrite, anatase, zircon, quartz and feldspar. The textural features of ores suggest that the bauxite has an authigenic origin but locally underwent transportation and re-deposition. Geochemical investigations indicate that the immobile elements like Al, Ti, Zr, Cr, Hf, Nb, Ta and Th were obviously enriched during bauxitization. Factors such as the type of parent rock, pH variation in weathering solutions, adsorption processes, groundwater chemical characteristics, Fe concentration variation in the weathering profiles, leaching degree of minerals, and geochemistry of elements have played a significant role in the distribution of trace and rare earth elements during weathering of the lateritic bauxite. The bauxites may have a close genetic relationship with the Hanjiadian mud shale and the Huanglong limestone in view of their similar chondrite-normalized REE patterns, Zr/Hf and Nb/Ta ratios. However, field observations and geochemical data suggest that the precursors of bauxites are complex and the main components of precursors are basic igneous rocks possibly from the Neoproterozoic basic igneous rocks and the Mesoproterozoic basic–ultrabasic intrusions in the Yangtze Block.

© 2013 Elsevier B.V. All rights reserved.

## 1. Introduction

According to the bedrock lithology, bauxite deposits can be commonly classified into two main categories: karstic bauxites that overly carbonate rocks regardless of the degree of karstification; and lateritic bauxites that overly aluminosilicate rocks (Bárdossy, 1982). Karst-type deposits originate from a variety of different materials, depending on the source area (Bárdossy, 1982). Lateritic bauxite is generally formed by in-situ lateritization, therefore, the most important factors in determining the extent and grade of it are thought to be the parent rock composition, climate, topography, drainage, groundwater chemistry and movement, location of the water table, microbial activity, and the duration of weathering processes (Bárdossy and Aleva, 1990; Grubb, 1963; Price et al., 1997). In addition, lateritic bauxites can be directly related to the underlying source rocks through their textures and compositions (Bárdossy and Aleva, 1990; Horbe and da Costa, 1999; Mutakyahwa et al., 2003). Although most of the known bauxite deposits are lateritic type, the geochemistry and genetic implications

of lateritic bauxite deposits have been rarely studied while the karstic bauxite deposits have been well examined (Bárdossy, 1982; Bárdossy and Kovács, 1995; Calagari and Abedini, 2007; Esmaeily et al., 2010; Karadag et al., 2009; Liaghat et al., 2003; MacLean et al., 1997; Taylor et al., 2008; Y. Liu et al., 2010; Zarasvandi et al., 2008, 2010). As a result, little is known to trace the precursors or reveal ore-forming process of lateritic bauxites.

Bauxite resources in China are abundant, ranking fifth in the world, after New Guinea, Australia, Brazil, and Jamaica. The bauxite deposits in China are mainly found in the Shanxi, Guizhou, Guangxi and Henan Provinces. Recently, huge quantities of lateritic bauxite ores have been discovered in Wuchuan, Zheng'an and Daozhen Counties, Northern Guizhou. As a result of research and exploration carried out in the Wuchuan–Zheng'an–Daozhen (WZD) region by Guizhou Nonferrous Metal Geological Exploration Bureau and Bureau of Geology and Mineral Exploration and Development of Guizhou Province, more than 20 lateritic bauxite deposits (Fig. 2) with more than 0.1 billion tons bauxite ores have been identified in the area, with several other unexplored districts also showing bauxite mineralization potential. Therefore, it is necessary to obtain detailed knowledge of geological, geomorphological settings and geochemistry of the known lateritic bauxite occurrences to shed

\* Corresponding author. Tel.: +86 851 5895900; fax: +86 851 5891664.  
E-mail address: [huangzhilong@vip.gyig.ac.cn](mailto:huangzhilong@vip.gyig.ac.cn) (Z. Huang).

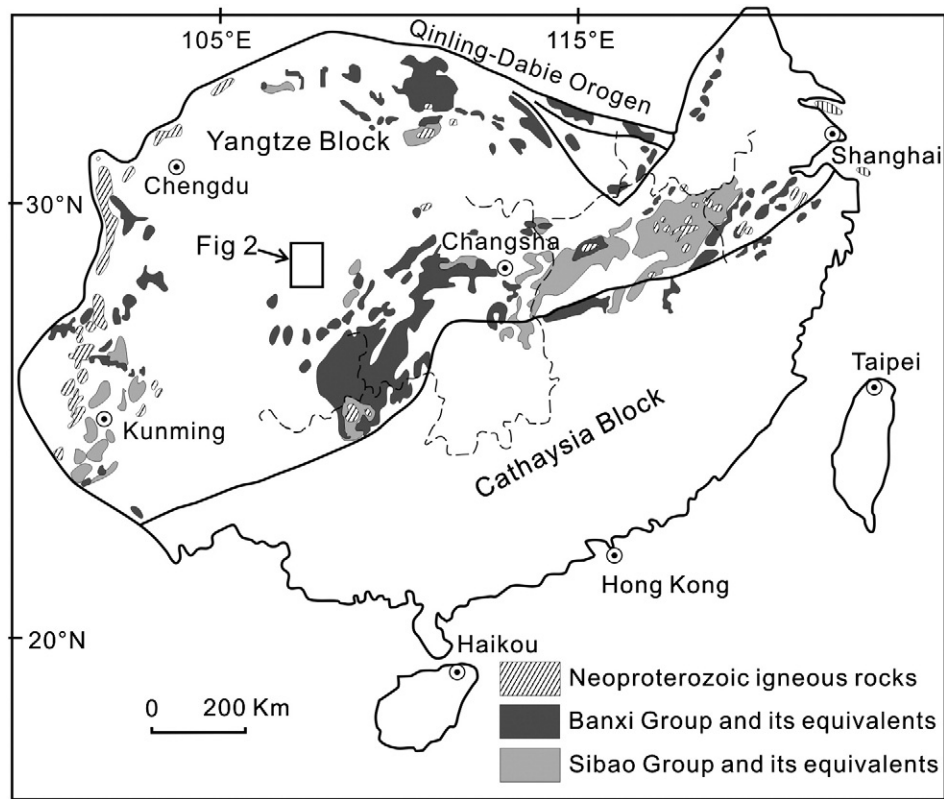


Fig. 1. Sketch map of geology in South China, with the distribution of Mesozoic to Neoproterozoic strata and magmatism within the Yangtze Block (modified after Wang et al., 2012b).

new lights on identifying other prospects for bauxite deposits in the WZD area.

Initial investigations have provided a first insight into the geology and conditions of lateritic bauxite deposits formation in the WZD area (Jin et al., 2009; Liu, 2007; Wu et al., 2006, 2008; X. Liu et al., 2010; Yin, 2009). However, the detailed ore-forming process is still ambiguous and the source rock of the WZD bauxite deposits has long been a matter of debate. The major and trace element geochemistry has proven to be a powerful tool in investigating various aspects of lateritic bauxite formation such as parent rock composition, diagenetic and epigenetic processes related to bauxitisation (Esmaily et al., 2010; MacLean et al., 1997; Mordberg, 1993). In this study, samples from four typical lateritic bauxite deposits in the WZD area were chosen to reveal more details of the ore-forming process and identify the precursor of the ores by considering the distribution of major and trace elements along with comprehensive geological, petrographical, mineralogical and geochemical characteristics of the deposits.

## 2. Geological settings

### 2.1. Regional geology

The South China Block consists of the Yangtze Block in the northwest and the Cathaysia Block in the southeast (Fig. 1). These two blocks came together to form the South China Block at ~1000–800 Ma during the assembly of the Rodinia supercontinent (Li and McCulloch, 1996; Li et al., 2009; Wang et al., 2006; Zheng et al., 2008). The oldest rocks exposed in the Yangtze Block are the 3.3–2.9 Ga Kongling TTG gneiss (Fan et al., 2013; Jiao et al., 2009; Qiu et al., 2000; Zhang et al., 2006). Neoproterozoic igneous rocks, such as TTG gneisses, granites, diorites, and gabbros, are widespread on the margins of the Yangtze Block (Fig. 1) (Li et al., 2002; Zhou et al., 2002). The meta-sedimentary basement of the southern Yangtze Block mainly consists of two low-grade

sequences separated by a regional angular unconformity, marking the boundary between the Mesoproterozoic and Neoproterozoic. Mesoproterozoic strata include bathy-abysal sandy-argillaceous terrigenous sediments with flysch bedding and metamorphosed mafic-ultramafic volcanic intercalations, such as tholeiite, spilite with pillow structure, and volcanoclastic rocks (BGMRCX, 1985; GXRGST, 1987, 1995), which are collectively termed as the Sibao Group in northern Guangxi Province, Lengjiayi Group in western Hunan Province, and Fanjingshan Group in Guizhou Province. The Neoproterozoic sedimentary strata named the Banxi Group in Hunan Province, the Danzhou Group in northern Guangxi Province, are mainly composed of sandstone, shale, conglomerate, pelite and lesser carbonate, spilite and volcanoclastic rock.

The WZD area is located near the southern margin of the Yangtze Block (Fig. 1). The exposed stratigraphic sequence in this area mainly consists of Cambrian, Ordovician, Silurian, Carboniferous, Permian, Triassic, Jurassic and Quaternary (Fig. 2). During Cambrian to Middle Silurian, the region experienced a large transgression–regression cycle under the influence of the first stage of Caledonian movement that resulted in the deposition of Cambrian to Silurian (GZBGMR, 1987). The oldest rock in the area is the Middle to Upper Cambrian dolomite of the Loushanguan Group (Fig. 3). The Ordovician consisted of dolomite, limestone and argillite and is overlain by the Lower–Middle Silurian Hanjiadian Group which is made up of grayish-green or purplish to reddish mud shale. During the Upper Silurian to Upper Carboniferous stage, a drop of sea level led to an epeirogenetic phase and exposed the Hanjiadian Group to intense weathering (GZBGMR, 1987). There are no outcrops of Upper Silurian, Devonian and Lower to Middle Carboniferous sediments in the area. The Upper Carboniferous limestone of the Huanglong Formation has been mostly eroded and occurred only at a few locations in this area. In the following transgression at the beginning of Middle Permian, the seawater submerged the weathered materials resulting in the deposition of the lateritic

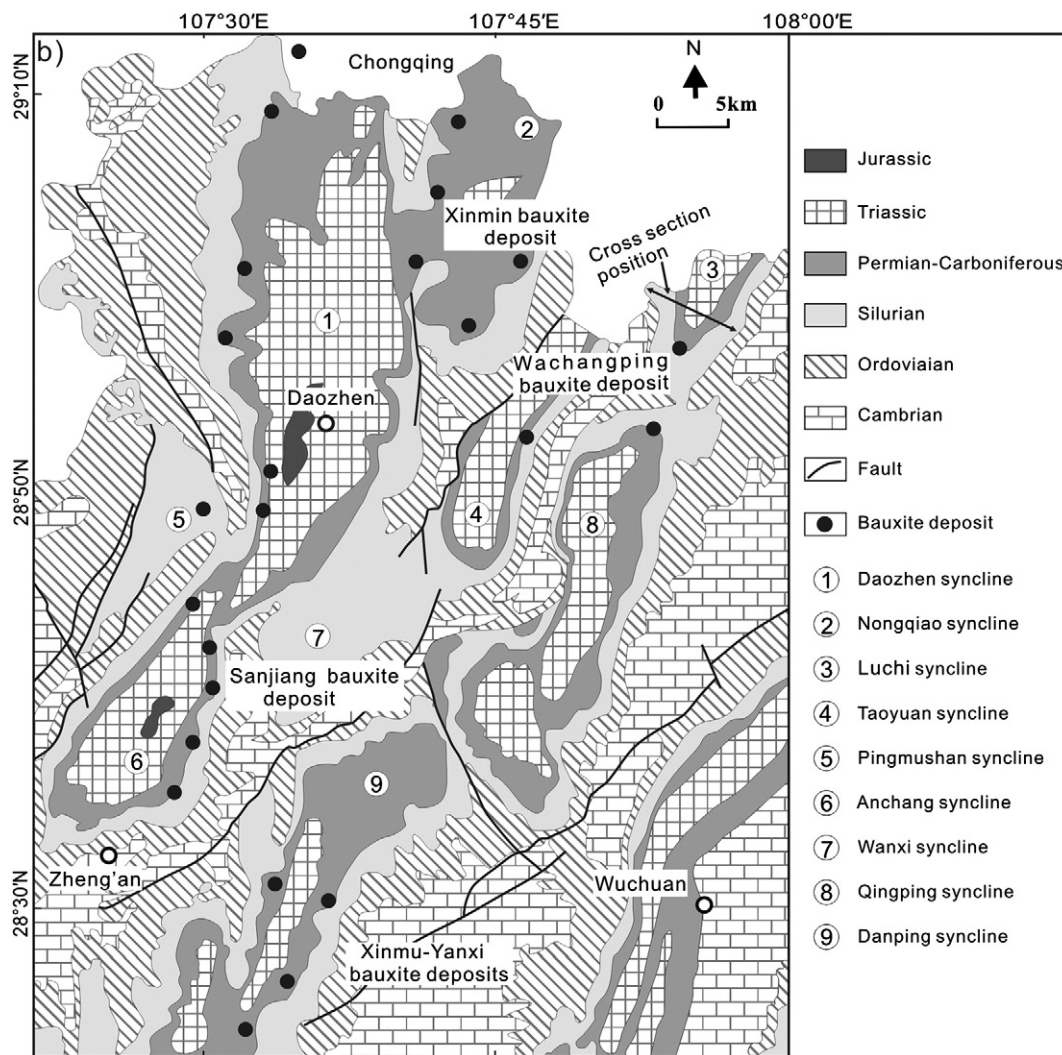


Fig. 2. Simplified geological map of the bauxite deposits in the WZD area (modified from Wu et al., 2008).

bauxite hosted in the Liangshan Formation which is approximately 5–17 m thick (Fig. 3). The Liangshan Formation is overlain by the Middle Permian limestone of the Qixia and Maokou Formation. Coal-rich Triassic consists of Dolomite, limestone, shale and sandstone and is overlain by Jurassic shale and sandstone.

The NNE-directed compression in this region resulted in widespread NNE-trending anticlinorium, synclinorium and faults (Fig. 2). The bauxitic horizons are strictly controlled by synclines and the ores are all hosted in limbs of the synclines (Fig. 2).

## 2.2. Local geology of bauxite occurrences

To study the geological and geochemical characteristics of the lateritic bauxite deposits in the WZD areas, four deposits (Wachangping, Xinmin, Sanjiang and Xinmu–Yanxi) in four synclines (Luchi, Nongqiao, Anchang and Danping) were selected to investigate the geological, petrographical and geochemical characteristics of these deposits. The Wachangping deposit, in the Luchi syncline, is the largest and most important bauxite deposit in the WZD area. It contains an estimated 44 million tons of bauxite ore with 40–79 wt.%  $\text{Al}_2\text{O}_3$  (Jin et al., 2009). The Nongqiao syncline hosts five bauxite deposits (Fig. 2) with the Xinmin bauxite deposit the largest one at an estimated 16 million tons of bauxite (Jin et al., 2009). The Anchang syncline hosts five bauxitic deposits in which the Sanjiang bauxite deposit is selected for sampling.

The Xinmu–Yanxi bauxite deposit in the northeastern limb of the Danping syncline is composed of the Xinmu, Wujiashi and Yanxi ore sections. Ore bodies of the Xinmu–Yanxi bauxite deposit are 1000–2500 m long and 3–10 m thick. The synclines and bauxitic horizons in the study area share similar geological and stratigraphic character. From the base upward, the synclines consists of mud-shales of the Hanjiadian Group, limestone of the Huanglong Formation, argillaceous and bauxitic rocks of the Liangshan Formation, marine limestone of the Qixia and Maokou Formations, limestone and marl of the Wujiaping and Changxing Formations, and argillaceous limestone and shale of the Yelang Formation. The ore bodies are controlled by strata, lithology and structure (Fig. 4). Based on their different compositions, three layers in the bauxitic horizons are distinguished (Fig. 5). The upper layer is gray and brown-gray in color and is composed of bauxite and bauxitic clay (UB); the middle layer is yellow-brown in color and is mainly composed of bauxite with a small amount of bauxitic clay (MB); and the lower layer is brick-red in color and is composed of laterites and ferritic bauxite (LB).

## 3. Sampling and analytical methods

In this study, 48 samples from the lateritic bauxite horizons (UB, MB, LB), Huanglong limestone (HL) and Hanjiadian mud shale (HS) in four representative lateritic bauxite deposits were collected for mineralogical and geochemical analysis. Samples X-1 to X-13 were

System		Formation(Fm.) and age	Thickness	Lithology and explanation
Mesozoic	Lower Triassic	Maocaopu Fm	550-690	Thick bedded limestone, dolostone and dolomitic limestone
		Yelang Fm	290-650	Limestone, argillite and shale
Upper Paleozoic	Upper Permian	Changxing Fm	40-70	Thick bedded limestone
		Wujiaping Fm	120-150	Limestone intercalated with siliceous rocks and argillite, containing coal
	Middle Permian	Maokou Fm	240-370	Massive limestone intercalated with dolomitic limestone
		Qixia Fm	90-180	Thick bedded limestone contain carbonaceous argillite
		Liangshan Fm	5-17	bauxite, bauxitic clay, laterite and carbonaceous argillite
		Huanglong Fm (Upper Carboniferous)	0-10	Massive limestone
Lower Paleozoic		Hanjiadian Group (Lower-Middle Silurian)	120-680	Silt mud shales
		Ordovician	470-600	Dolostone, limestone and argillite
		Loushanguan Group (Middle-Upper Cambrian)	>1000	Thick bedded dolostone intercalated with argillaceous dolostone
				Angular unconformity

Fig. 3. Stratigraphic columnar section of the study area.

collected from the Xinmin deposit; samples W-1 to W-15 were collected from the Wachangping deposit; samples S-2 to S-9 were collected from the Sanjiang deposit; and samples Y-1 to Y-11 were from the Xinmu–Yanxi deposit. In addition, all the samples were collected from the bottom upward of drill cores, outcrops and profiles.

For whole-rock geochemical analyses the samples were crushed to 200-mesh using an agate mill. All analyses were carried out at the State Key Laboratory of Ore Deposit Geochemistry (SKLOGD), Institute of Geochemistry, Chinese Academy of Sciences (IGCAS). Major elements

were determined by a wet chemistry method using the parallel samples and international standard samples for data quality control, with precision better than 5%. Trace elements were analyzed using a Perkin-Elmer ELAN-DRC-e ICP-MS. The powdered samples (50 mg) were dissolved in high-pressure Teflon bombs for 48 h at ~195 °C using HF + HNO<sub>3</sub> mixture. Rh was used as an internal standard to monitor signal drift during counting (Qi et al., 2000). The international standards GBPG-1, OU-6, and the Chinese national standard GSR-3 were used for analytical quality control, with the precision generally better than 5%.

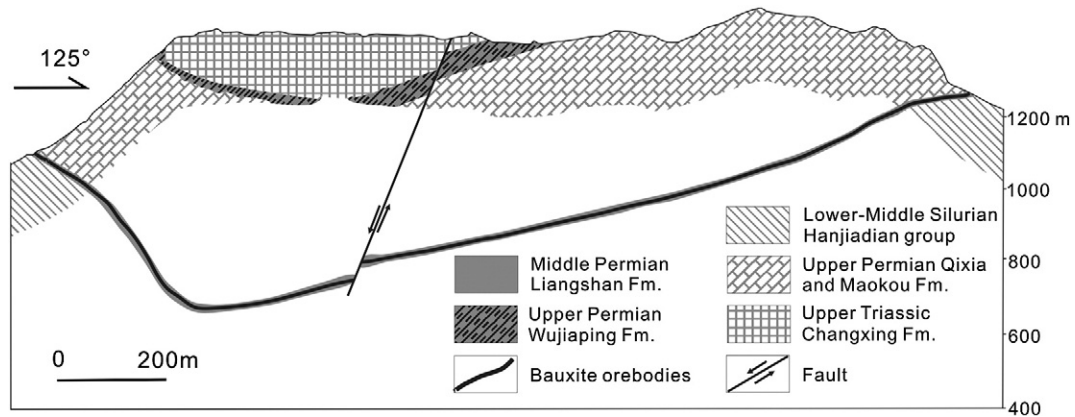


Fig. 4. Cross-section of the Wachangping bauxite deposit (for position see Fig. 2).

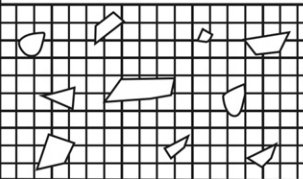
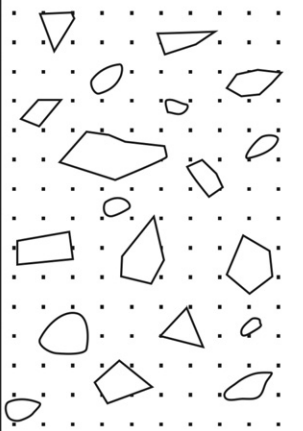
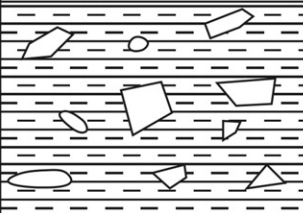
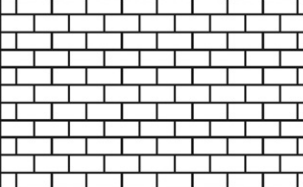
Stratigraphic columns	Thickness(m)	Lithologic feature
	0-2.8	Clastic bauxite and bauxitic clay with small amount of carbonaceous shale
	0-10	Oolitic-pisolitic, pelitomorphous bauxite and few bauxitic clay
	0-4	laterite and bauxitic argillite with small amount of ferritic bauxite
	0-5	Limestone

Fig. 5. Sketch map of a stratigraphic column of the bauxitic horizons of the bauxite deposits in the WZD area.

Mineralogical studies of the samples were carried out using the X-ray diffraction (XRD) and scanning electron microscope (SEM) analyses at SKLOGD. X-ray diffraction is used to obtain the semi-qualitative mineralogical compositions. X-ray diffraction patterns were obtained on randomly oriented powder specimens using a D/MAX-2000 diffractometer with Cu K $\alpha$  ( $\lambda = 1.5406 \text{ \AA}$ ) radiation at a voltage of 56 kV and a current of 182 mA. SEM analyses were done with an EPMA-1600 scanning electron microscope using Genesis EDAX. Back scattered electron images were obtained at an accelerating voltage of 120 kV and a beam current of  $\sim 10 \mu\text{A}$ .

## 4. Results

### 4.1. Mineralogy and texture

Mineralogical compositions are essentially similar in all of the bauxitic–lateritic occurrences in the WZD area. Detailed textural and mineralogical analysis based on optical microscopy, XRD and SEM data, which revealed that diasporite, boehmite, kaolinite, smectite, illite and hematite are the major mineral components in the bauxite ores; gibbsite, chlorite, pyrophyllite, goethite, pyrite and anatase are minor minerals; lesser quantities of the other minerals such as zircon,

rutile, calcite, quartz, feldspar, limonite, dolomite and calcite also have been found (Table 1). Gibbsite, boehmite and diasporite are the major aluminum phases in bauxites and laterites. Among them, gibbsite is the principal component in tropical bauxites formed in areas characterized by a hot rainy climate with alternating dry

Table 1  
Semi-quantitative mineralogical analyses of typical bauxite samples (wt.%).

Sample	W-1	W-2	W-3	S-3	S-4	X-1	X-5	X-8
Diasporite	68.60	87.60	45.49	1.57	2.40	91.21	16.18	56.87
Boehmite	0.15	Y	Y	94.50	88.96	–	67.69	3.00
Kaolinite	21.65	4.71	3.61	0.46	3.88	0.24	5.25	–
Illite	0.17	1.42	22.43	1.82	0.43	–	0.22	23.15
Iron minerals	2.40	0.72	2.62	Y	Y	6.10	0.46	0.47
Smectite	3.26	1.15	5.76	–	1.00	–	3.66	1.28
Quartz	0.30	0.88	7.18	1.65	2.11	–	–	5.42
Anatase	Y	Y	4.16	Y	Y	2.45	–	Y
Chlorite	–	–	–	–	–	–	2.62	6.45
Feldspar	3.47	–	2.77	–	–	–	–	3.36
Calcite	–	–	4.06	–	1.22	–	–	–
Gibbsite	–	–	–	–	–	–	3.92	–

Y represents mineral phases that have been identified by XRD, but their normative values cannot be calculated due to their very low abundances.

periods. However, bauxites with mainly boehmite seem to be more restricted to the subtropical areas (Kloprogge et al., 2002). Direct precipitation of diaspore from A1 solutions has rarely been observed (Peryea and Kittrick, 1988). If the gibbsite is hydrothermally treated at a higher pressure, diaspore is likely to form. Chen et al. (1995) prepared pure diaspore samples by the dehydration of gibbsite at a temperature of 623 K and a pressure of  $1.5 \times 10^5$  Pa.

The fine-grained mineral constituents in the bauxite ores can hardly be identified under the microscope. Therefore, petrographic investigations were mainly focused on textural features. The main textures of the bauxite ores in the studied area are pelitomorphic, oolitic–pisolitic and clastic (Fig. 6a, b, c and d). Spherical grains such as ooids and pisoids are important components in most ore samples (Fig. 6a, c, d and f). The presence of ooids and pisoids can be attributed to the heterogeneity of the initial colloids that were derived from alteration of source rocks. Mineral components of the matrix in the bauxite ores are cryptocrystalline diaspore, hematite, kaolinite and chamosite. A small amount of euhedral–hypidiomorphic diaspore occurs in the matrix of the bauxite

ores although most of the diaspores are cryptocrystalline (Fig. 6e). The most important silicate minerals that accompany diaspore are kaolinite and minor quartz. Chamosite mainly coexists with diaspore (Fig. 7a), suggesting that the chamosite principally formed in a reducing environment (Liu et al., 2012; Temur, 2006). In some samples, fractured and corroded quartz grains are embedded in a matrix of chamosite, diaspore and kaolinite (Fig. 7b). Relict minerals are principally altered plagioclase and amphibole (Fig. 7c).

Ooids of various shapes and sizes, broken pisolites, and flattened nodules indicate re-depositional conditions (Fig. 6c). The fractures within individual ooids and cutting through the matrix are further important epigenetic features of the deposit (Fig. 6f). Various fractures, joints, and veinlets are filled with materials such as hematite, goethite, pyrite, magnetite/maghemite etc (Fig. 7d and e). Veinlets of iron oxides are common suggesting redistribution of Fe in the weathered profile (Calagari and Abedini, 2007). Part of zircon grains (Fig. 7f) shows sub-rounded edges and fractures, also indicating that the partial weathered materials experienced locally transportation.

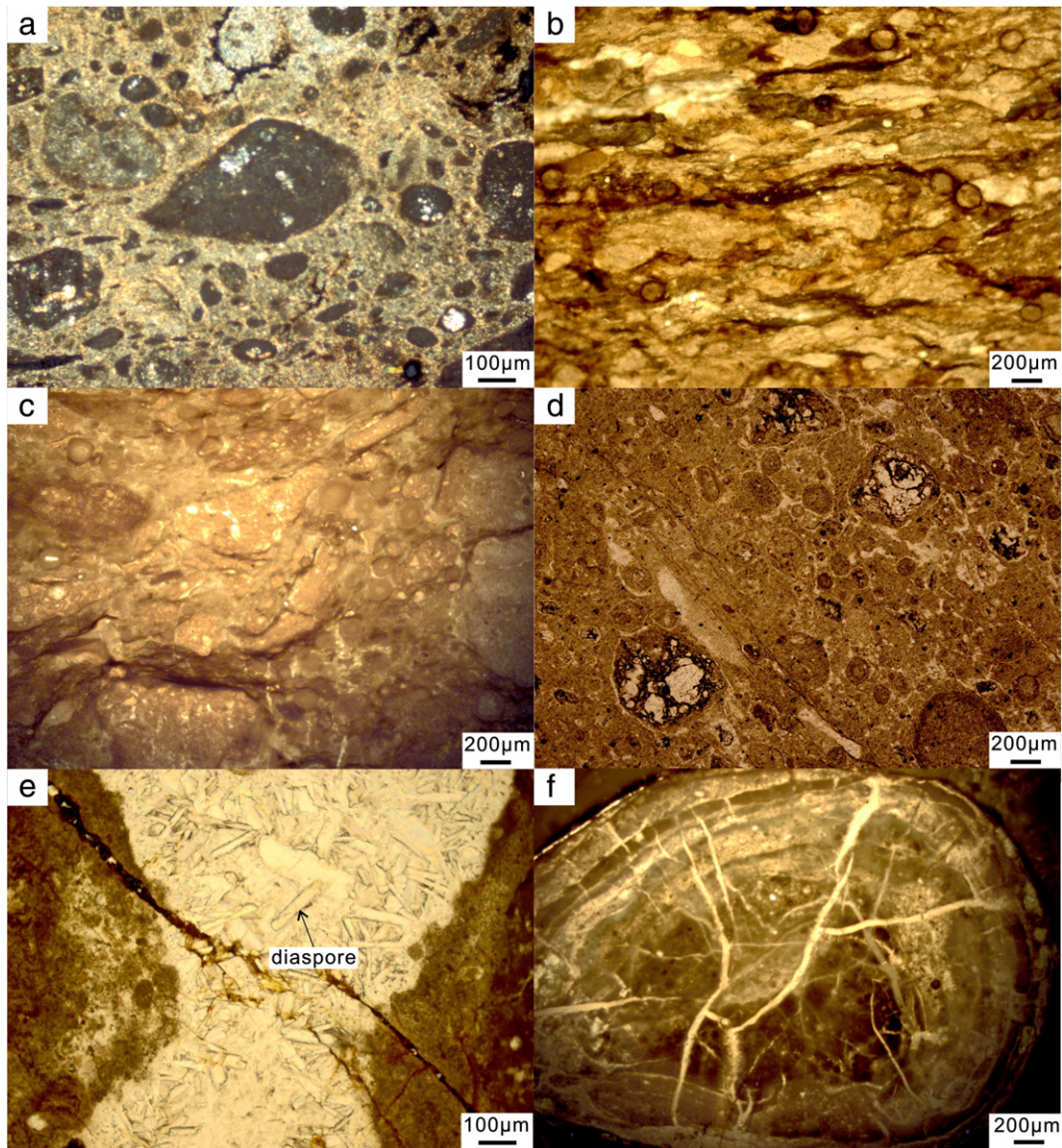


**Fig. 6.** Microphotographs of bauxite ores under plane-polarized light. a) Oolitic texture with ferruginous ooids of various shapes and sizes; b) pelitomorphic texture; c) broken pisolites and the flattened nodules indicate depositional conditions; d) clastic texture with few diaspore-cemented intraclasts. e) euhedral–hypidiomorphic diaspore; and f) the fractures within individual ooids.

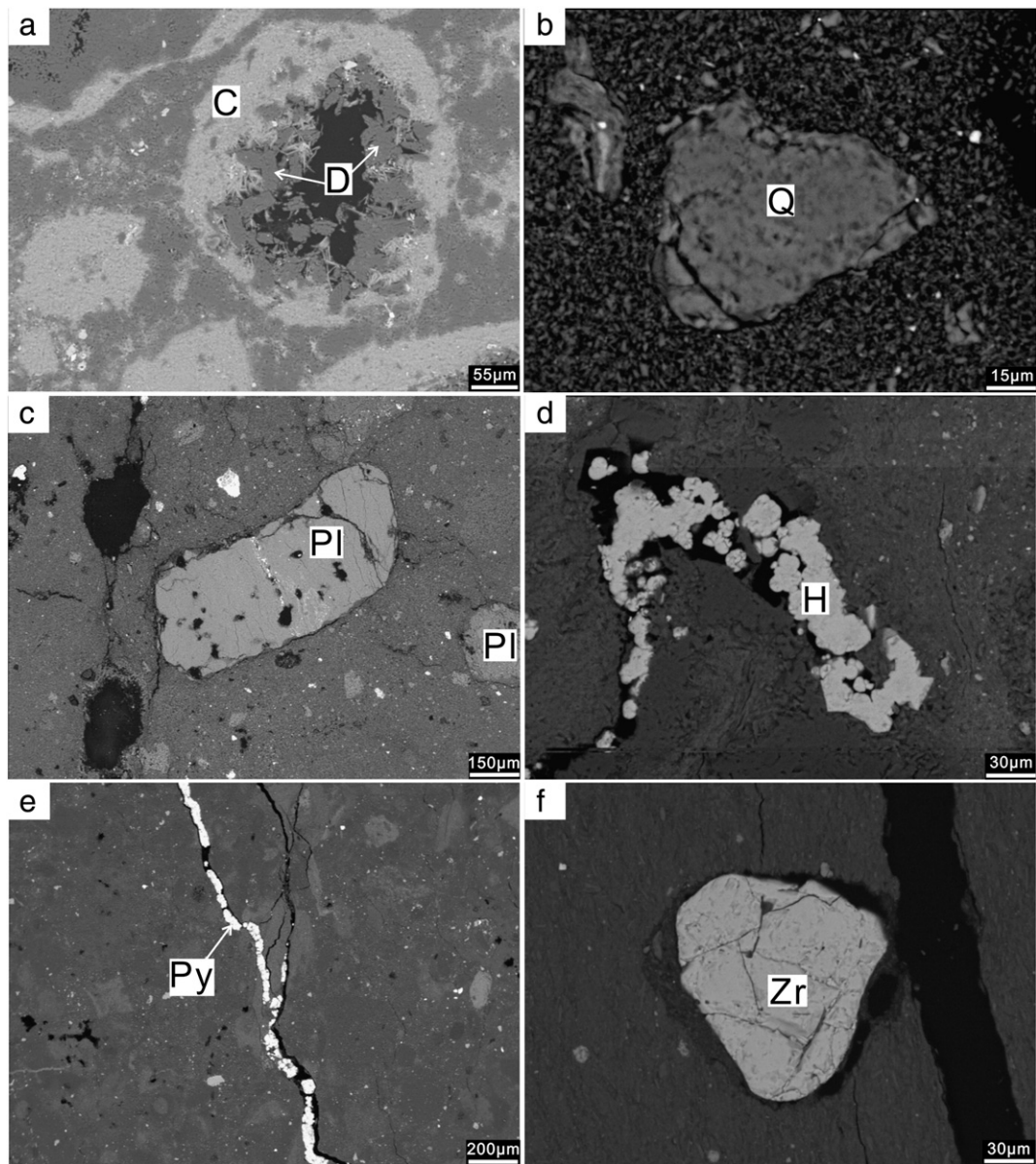


**Fig. 7.** Backscatter electron (BSE) micrographs of bauxite ores. a) An ooid formed by a diaspore core and a cortex of chamosite within a matrix that is mainly composed of chamosite and diaspore; b) fractured and corroded quartz grains are embedded in a matrix of diaspore, iron oxides, and kaolinite; c) relict plagioclase scattered within diaspore matrix; d) granular hematite filling in the void space in the ore; e) pyrite filling in the veinlet in the ore; and f) zircon scattered within diaspore matrix show sub-rounded edges and fractures. (C = chamosite; D = diaspore; Q = quartz; Pl = plagioclase; H = hematite; Py = pyrite; Zr = zircon).

## 4.2. Geochemistry

The major, trace and rare earth element contents of the representative samples from the bauxitic deposits are given in Table 2.

### 4.2.1. Major elements

The ores are mainly composed of  $\text{Al}_2\text{O}_3$  (31–76 wt.%),  $\text{SiO}_2$  (1.9–47 wt.%),  $\text{Fe}_2\text{O}_3$  (0.6–26.6 wt.%), and  $\text{TiO}_2$  (0.4–3.1 wt.%) with LOI ranging from 5.6 wt.% to 15.3 wt.%. Alkalis and alkali earth elements show low values, probably because these elements are highly mobile and are usually leached out during chemical weathering. The enhanced  $\text{Fe}_2\text{O}_3$  contents in the lower horizon are attributed to the presence of iron minerals like hematite and goethite formed under suitable Eh–pH conditions during the lateritic weathering processes. Among the major elements,  $\text{Al}_2\text{O}_3$  and  $\text{TiO}_2$  showed the highest positive correlation, while  $\text{Al}_2\text{O}_3$  and  $\text{SiO}_2$  display a negative correlation (Fig. 8). These patterns are consistent with leaching of silica and

residual enrichment of aluminum and titanium during chemical weathering.

The triangular variation diagrams of  $\text{Al}_2\text{O}_3$ – $\text{SiO}_2$ – $\text{Fe}_2\text{O}_3$  are commonly used to show the degree of lateritization, mineral control and bauxite classification. Based on the mineralogical classification of Aleva (1994), most of the bauxite samples in the studied areas fall within the bauxite and kaolinitic bauxite fields (Fig. 9). Nevertheless, Fig. 10 indicates that chemical variability is process-related and can be explained by different degrees of the lateritization, so that  $\text{SiO}_2$ -rich samples experienced weak lateritization while  $\text{Al}_2\text{O}_3$ -rich composition is indicative of a higher degree of lateritization (Meyer et al., 2002).

### 4.2.2. Trace elements

In general, trace elements such as Zr, V, Nb, Cr, Y, Ga and Th are enriched in the bauxitic profiles. Zr ranges from 175 to 869 ppm. V and Cr are above 100 ppm with the exception of X-3. Nb, Y, Ga and Th are in the tens of ppm range. Other trace elements range from less

than 1 ppm to tens of ppm (Table 2). The upper continental crust (UCC)-normalized trace element patterns of the bauxite horizons show quite similar characteristics such as depletion peaks for Ba, Sr and K, and enrichment peaks for Zr, Hf, Ti, Th, U, Ta and Ce (Fig. 11). However, samples of LB were enriched in La and Ce relative to MB and UB. Correlation analyses for the bauxite samples revealed that Zr vs. Nb and Zr vs. Ta display positive correlation (Fig. 12). Furthermore, Zr vs. Hf and Nb vs. Ta display the highest positive correlation with correlation coefficients ( $R^2$ ) of 0.99 and 0.97, respectively (Fig. 12). These reflect that elements such as Zr, Hf, Nb and Ta show similar geochemical behavior and were immobile during the process of bauxitization in the WZD bauxite deposits.

Similar decreasing trends occur in the  $\Sigma$ REE,  $\Sigma$ LREE and  $\Sigma$ HREE contents and  $\Sigma$ LREE (La–Sm)/ $\Sigma$ HREE (Gd–Lu) ratios of the bauxite samples from bottom to top of the bauxite profiles (Table 2, Fig. 13). The LB has the highest  $\Sigma$ REE (from 120 ppm to 847 ppm) and  $\Sigma$ LREE (La–Sm)/ $\Sigma$ HREE (Gd–Lu) ratios (from 4.9 to 19.7). The MB has higher  $\Sigma$ REE (from 53 ppm to 122 ppm) and  $\Sigma$ LREE (La–Sm)/ $\Sigma$ HREE (Gd–Lu) ratios (from 1.4 to 6.9). The UB has low  $\Sigma$ REE (from 13 ppm to 52 ppm) and  $\Sigma$ LREE (La–Sm)/ $\Sigma$ HREE (Gd–Lu) ratios (from 0.6 to 3.6). The Y contents of the bauxite samples also display decreasing trend from bottom to top of the profiles (Table 2). The  $\Sigma$ REE content (from 184 ppm to 212 ppm) and  $\Sigma$ LREE (La–Sm)/ $\Sigma$ HREE (Gd–Lu) ratios (from 7 to 10.6) of the mud shales in the Hanjiadian Group are higher than those of UB and MB and lower than those of LB. However, limestones in the Huanglong formation are characterized by low  $\Sigma$ REE contents (10.2–20.2 ppm). The chondrite-normalized REE patterns of the bauxite horizons, Hanjiadian mud shales and Huanglong limestones show quite similar signatures such as enriched LREE, depleted HREE, relatively flat HREE and visible Eu anomalies varying between 0.46 and 0.97 (Table 2, Fig. 13). However, they differ in  $\Sigma$ REE and Ce anomalies. Most of bauxite horizons samples show positive Ce anomalies with exception of few samples in LB, whereas the Hanjiadian mud shales are characterized by weak negative or no Ce anomalies, and Huanglong limestones show negative Ce (Table 2, Fig. 13).

## 5. Discussion

### 5.1. Parental affinity

Elements like Ti, Zr, Nb, Th, Ta, Hf, Ga, Cr and Ni have been used to identify parent rocks for bauxite and follow the various stages of the bauxitization process (Calagari and Abedini, 2007; Liaghat et al., 2003; Maclean, 1990; MacLean et al., 1997; Y. Liu et al., 2010) because they are considered to be immobile during the weathering processes (Andrews et al., 2001; MacLean and Barrett, 1993; Maclean and Kranidiotis, 1987; MacLean et al., 1997; Panahi et al., 2000; Y. Liu et al., 2010). Moreover, MacLean et al. (1997) proposed that the immobile elements can even be used to trace the source of aluminum to a particular rock type or unit. In the Ni–Cr diagram (Fig. 14), most of the WZD bauxite sample plots are through lateritic bauxite field with a mixed precursor of basalt and shale.

The ratios of immobile elements (e.g., Zr/Hf ratios) in bauxite can also be used to identify source rocks (Calagari and Abedini, 2007). These ratios when plotted in cross plots produce linear arrays with high correlation that pass through the origin of the plot belonging to parent rock(s) (Maclean, 1990). Both the Zr–Hf and Nb–Ta diagrams create a highly correlated single array for the bauxites, Huanglong limestone and Hanjiadian mud shale that passes through the origin (Fig. 15), indicating that the samples are genetically related. In addition, REE patterns can also be used to identify source materials (Esmaeily et al., 2010). Therefore, the similarities of the REE patterns and Eu anomalies of the bauxite ores, Hanjiadian mud shale and Huanglong limestone imply the same source for them. These relationships are explicable when considering transgressive deposition of the Huanglong Formation on the depression of the Hanjiadian mud shale. Simultaneously, the

Hanjiadian mud shale shows a negative Eu anomaly that was most likely inherited from the basic precursor rocks as a consequence of breakdown of feldspars (Galan et al., 2007; Karadag et al., 2009; Villaseca et al., 2003). Eu anomalies range from 0.46 to 0.97 in the bauxite horizons and Huanglong limestone may also be related to the weathering of Hanjiadian mud shale.

Sometimes, the regional strata can provide some materials for the bauxite (Wang et al., 2012a). Although the geochemical data for the bauxite ores and Hanjiadian mud shale suggest basic igneous rocks as a main component of their source material, there is no direct field evidence for such a rock in the region and in the surrounding areas. It is therefore supposed that some old buried Precambrian rock of basic provenance, probably the Neoproterozoic basic igneous rocks and the basic-ultrabasic volcanic intercalations from the Mesoproterozoic strata of the southern Yangtze Block, could have been the precursor of them. This is further supported by similar geochemical signatures of WZD bauxite ores and these basic igneous rocks (Li et al., 2002; Yan et al., 1995; Zhou et al., 2004, 2009).

### 5.2. Controlling factors of the trace element distribution

The enrichment and depletion of the trace elements are related to their carrier mineral phases in the source rock (Meshram and Randive, 2011). Therefore, even very mobile elements can be enriched in bauxite profiles if their host minerals have not been dissolved (Meshram and Randive, 2011). A strong negative Sr anomaly in the UCC-normalized trace element patterns of the bauxite horizons (Fig. 11) resulted from unmixing of feldspars. Similarly, Zr is generally known to be relatively immobile during weathering due to the high weathering resistance of zircon (Mordberg and Spratt, 1998), the distinct positive anomaly of Zr therefore indicates the enrichment of zircon in the source rocks.

In general, weathering of the minerals of the parent rocks causes mobilization of elements and fractionation of LREE and HREE, as well as Ce and Eu anomalies (Hill et al., 2000; Karadag et al., 2009; MacLean et al., 1997). In addition, REE is released from primary minerals and absorbed by or adsorbed onto all types of minerals and amorphous surface coatings during kaolinization and lateritization (Karadag et al., 2009). Therefore, carrier minerals contained in the bauxite may be an important factor to affect the leaching degree of the rare earth elements. Many kinds of minerals have been identified to be potential hosts for REEs. They include clay minerals (Condie, 1991), phosphate minerals (e.g., apatite) (Braun et al., 1993), Mn-oxides and hydroxides (Koppi et al., 1996; Mutakyahwa et al., 2003), and Fe-oxides and hydroxides (Pokrovsky et al., 2006). In the bauxite ores in the WZD region, REE is positively correlated with Si ( $r = 0.01$ – $0.4$ ), Fe ( $r = 0.3$ – $0.5$ ), Na ( $r = 0.1$ – $0.5$ ) and Ca ( $r = 0.3$ – $0.7$ ) (Table 3), which together with chemical composition and statistical data (Tables 1 and 2), suggest that REE distribution in the bauxite horizons is mainly controlled by clay minerals and iron minerals such as goethite. Accordingly, REE may easily get adsorbed at the surface of clay minerals such as kaolinite and smectite, which seems to be important in forming the geochemical cycle of these elements (Laufer et al., 1984; Roaldset, 1979). In addition, the positive correlation between  $\Sigma$ REE and  $\text{Fe}_2\text{O}_3$  in bauxite ores in the WZD region is consistent with the fact that goethite acts as an important scavenger for REE especially LREE (Kühnel, 1987; Mameli et al., 2007; Mongelli, 1997), which is a reasonable explanation for the enrichment of REE and fractionation of LREE over HREE observed in the lower Fe-rich horizon. This points to the importance of Fe-minerals in controlling REE distribution and the shape of chondrite-normalized REE patterns for bauxite. On the other hand, the presence of authigenic REE minerals can significantly influence the shape of the REE pattern of bauxite ores as been demonstrated in several studies of bauxite deposits where the REE mostly occurs as various authigenic REE minerals (Boulange et al., 1996; Calagari and Abedini, 2007; Mordberg and Nesterova, 1996; Wang et al., 2010). Therefore, the possibility of the presence of authigenic REE minerals in the lower bauxitic layer could



**Table 2**  
Major (in wt. %), trace and rare earth elements (in ppm) data of the representative samples from the study area.

Layer	UB											MB												
	Sample	X-1	X-2	X-3	X-4	W-1	W-2	W-3	S-1	S-2	S-3	Y-1	X-5	X-6	X-7	W-4	W-5	W-6	W-7	S-4	S-5	Y-2	Y-3	Y-4
SiO <sub>2</sub> (wt.%)	4.19	8.45	43.56	4.21	1.90	16.18	30.29	43.96	2.00	13.82	15.29	28.40	42.35	15.02	10.72	40.06	47.30	45.60	17.85	18.02	1.70	1.60	41.36	40.41
Al <sub>2</sub> O <sub>3</sub>	76.35	71.25	38.17	72.25	71.63	55.32	51.28	36.56	66.07	65.23	64.12	49.62	34.20	42.89	59.20	36.39	40.20	36.05	60.00	58.23	71.52	71.06	36.52	35.66
TiO <sub>2</sub>	3.12	3.02	0.65	3.12	3.06	2.53	2.25	0.57	2.85	2.86	2.76	1.75	0.64	1.67	2.11	1.02	1.18	1.08	2.42	2.65	3.02	3.10	1.15	0.86
Fe <sub>2</sub> O <sub>3</sub>	1.32	1.37	1.36	5.98	6.67	7.75	1.42	3.75	6.95	2.07	1.43	2.72	6.63	26.58	12.79	4.78	0.60	1.05	2.43	3.35	6.02	5.81	4.75	4.74
Na <sub>2</sub> O	0.18	0.17	0.67	0.08	1.06	0.28	1.05	0.71	1.64	1.61	1.73	1.37	0.47	0.56	0.06	0.61	0.57	0.39	1.28	1.31	0.95	1.21	1.79	0.84
K <sub>2</sub> O	0.12	0.23	0.29	0.10	0.20	0.18	1.93	4.72	0.46	1.07	1.34	0.48	0.44	0.11	0.25	0.65	0.28	0.27	0.86	0.84	0.32	0.34	2.40	0.69
CaO	0.28	0.44	0.22	0.31	0.36	0.27	0.39	0.17	0.16	0.11	0.20	0.34	0.48	0.21	0.46	1.06	0.74	0.55	0.15	0.20	0.40	0.39	0.20	0.15
MgO	0.06	0.42	0.83	0.06	0.51	3.25	0.57	1.06	3.94	0.49	0.51	1.17	0.30	1.48	0.82	0.44	0.56	0.30	1.71	1.90	1.10	1.34	0.92	2.87
MnO	0.01	0.01	0.02	0.01	0.01	0.01	0.01	0.02	0.56	0.01	0.01	0.02	0.01	0.05	0.05	0.00	0.02	0.02	0.01	0.01	0.01	0.37	0.02	0.01
P <sub>2</sub> O <sub>5</sub>	0.06	0.06	0.08	0.07	0.10	0.09	0.10	0.07	0.12	0.08	0.10	0.10	0.10	0.08	0.04	0.04	0.12	0.12	0.06	0.07	0.10	0.12	0.14	0.12
LOI	14.15	14.05	14.02	13.75	14.29	13.94	10.76	8.26	15.32	12.48	12.32	14.08	14.20	11.13	13.67	15.17	8.30	14.40	13.35	13.32	14.66	14.50	10.48	13.54
Total	99.84	99.83	99.86	99.93	99.79	99.80	100.05	99.85	100.07	99.82	99.81	100.05	99.82	99.78	100.08	100.22	99.87	99.83	100.12	99.90	99.80	99.84	99.72	99.89
Rb (ppm)	0.48	6.54	4.25	0.63	4.21	4.64	115	190	7.74	52.3	58.9	9.70	22.7	0.56	0.15	14.7	209	4.11	36.4	32.2	8.88	10.8	96.0	28.8
Ba	4.65	23.3	14.2	5.05	38.4	22.5	369	248	39.0	144	119	55.2	55.8	52.4	101	123	873	39.4	94.8	93.0	114	82.7	132	48.4
Th	25.3	19.3	11.0	27.7	49.1	39.9	43.3	15.0	120	22.7	30.8	51.9	19.8	88.3	64.6	36.2	24.8	22.1	30.3	42.6	84.0	96.0	23.5	59.9
U	12.7	22.2	5.47	18.8	23.6	9.73	14.2	6.39	7.23	14.0	8.93	12.1	7.33	10.5	10.3	7.40	7.39	7.75	8.37	6.30	16.8	15.4	4.12	5.24
Ta	4.57	4.03	2.10	4.45	4.65	4.16	4.58	0.96	3.50	2.43	3.79	3.19	1.97	3.91	4.73	2.51	2.70	3.42	2.83	3.91	3.58	3.50	2.39	3.48
Nb	62.1	55.8	31.0	59.1	63.6	58.6	59.3	13.5	46.1	31.7	50.6	43.8	28.2	54.8	59.9	31.0	33.3	41.5	36.4	52.1	50.4	48.6	32.7	46.9
Sr	9.85	12.8	26.0	7.40	50.2	32.0	62.6	69.0	58.7	72.9	48.1	106	80.3	184	80.1	134	124	24.5	58.8	37.8	110	162	122	163
Y	11.5	15.1	7.69	22.3	21.9	23.7	23.2	10.9	43.6	14.0	22.7	21.3	16.5	39.3	38.2	32.9	15.9	23.5	22.0	36.9	34.6	42.0	20.7	32.7
Zr	647	575	339	669	844	729	599	175	680	306	566	608	414	701	597	349	321	869	370	597	693	715	287	586
V	430	335	95	371	365	296	294	169	343	310	311	360	370	418	305	148	144	231	267	280	322	334	205	230
Cr	144	115	87	133	372	217	166	117	539	110	146	328	194	501	368	150	162	230	129	297	465	520	187	286
Ni	2.15	26.1	5.82	3.22	1.56	14.0	18.2	2.05	69.5	17.9	17.5	31.6	3.26	40.9	10.3	121.4	1.58	38.0	17.5	39.6	3.07	3.09	83.6	65.2
Ga	47.6	62.3	9.04	70.0	116	64.2	35.1	13.3	107	26.5	34.5	36.6	17.8	106	85.4	25.1	27.5	32.4	27.9	101	101	91.9	22.6	53.4
Hf	17.8	15.9	8.26	18.3	23.3	19.1	16.4	4.76	17.2	8.69	15.4	17.0	11.0	19.0	16.1	9.49	8.84	22.8	10.4	15.9	19.4	19.8	7.66	16.0
La	1.42	0.89	2.96	0.90	2.01	5.14	5.22	2.09	2.58	5.44	5.33	7.98	12.9	14.2	12.1	13.8	10.1	9.77	5.00	7.26	5.71	10.0	13.1	7.13
Ce	3.63	2.37	9.23	3.65	8.46	15.9	12.5	6.62	12.8	22.1	20.8	32.2	40.7	59.4	49.9	34.2	29.8	21.4	21.3	15.0	22.5	35.2	65.1	41.9
Pr	0.35	0.23	0.79	0.33	0.92	1.66	1.08	0.74	0.86	2.06	1.82	2.88	4.04	3.99	3.38	3.86	2.82	2.24	1.91	2.11	2.46	4.06	2.75	2.29
Nd	1.46	1.03	2.82	1.47	3.94	6.78	3.89	3.67	4.02	7.49	6.69	11.5	15.8	15.5	12.8	15.2	9.08	8.43	6.83	8.33	10.1	16.3	9.89	9.67
Sm	0.55	0.53	0.68	0.69	1.39	1.62	1.23	1.19	1.61	1.76	1.93	3.30	2.46	4.03	3.18	3.65	1.58	1.81	1.97	2.78	3.03	4.39	2.35	2.72
Eu	0.22	0.22	0.16	0.26	0.58	0.45	0.39	0.34	0.61	0.52	0.60	0.94	0.36	1.07	0.82	0.84	0.41	0.32	0.59	0.62	1.05	1.34	0.53	0.64
Gd	1.05	1.29	0.83	1.79	2.33	2.60	2.02	1.25	4.11	1.82	2.51	3.32	2.22	4.94	4.16	3.38	1.89	2.15	2.61	3.76	4.16	5.21	2.79	3.76
Tb	0.24	0.32	0.18	0.46	0.53	0.55	0.54	0.31	0.94	0.43	0.60	0.65	0.42	0.92	0.86	0.84	0.39	0.48	0.64	0.94	0.90	1.07	0.50	0.77
Dy	1.75	2.19	1.24	3.41	3.65	3.66	3.92	2.00	6.68	2.85	4.17	4.17	2.62	6.02	5.65	6.65	2.71	3.54	4.32	6.68	5.97	7.08	3.49	5.22
Ho	0.44	0.54	0.29	0.83	0.82	0.88	0.98	0.43	1.58	0.65	1.00	0.93	0.65	1.43	1.33	1.65	0.59	0.77	0.98	1.63	1.34	1.60	0.87	1.21
Er	1.29	1.56	0.84	2.21	2.32	2.56	3.03	1.17	4.48	1.82	2.80	2.65	2.01	4.30	4.00	5.00	1.92	2.48	2.75	4.87	3.66	4.39	2.71	3.47
Tm	0.20	0.24	0.12	0.33	0.34	0.41	0.47	0.18	0.64	0.30	0.44	0.42	0.31	0.66	0.64	0.84	0.32	0.38	0.43	0.76	0.53	0.66	0.44	0.54
Yb	1.46	1.78	0.94	2.23	2.43	2.95	3.47	1.18	4.51	2.04	3.17	3.00	2.18	4.71	4.72	6.34	2.25	2.82	3.00	5.10	3.70	4.41	3.25	3.72
Lu	0.21	0.25	0.14	0.33	0.36	0.43	0.49	0.16	0.67	0.30	0.47	0.41	0.32	0.72	0.65	0.89	0.33	0.40	0.44	0.78	0.51	0.64	0.49	0.55
ΣLREE	7.41	5.06	16.5	7.04	16.7	31.1	23.9	14.3	21.9	38.9	36.6	57.9	75.9	97.1	81.3	70.7	53.4	43.7	37.0	35.5	43.8	67.0	93.2	63.7
ΣHREE	6.86	8.39	4.74	11.8	13.4	14.5	15.3	7.02	24.2	10.7	15.8	16.5	11.1	24.8	22.8	26.4	10.8	13.3	15.8	25.1	21.8	26.4	15.1	19.9
ΣLREE/ΣHREE	1.08	0.60	3.48	0.59	1.25	2.15	1.56	2.04	0.90	3.62	2.32	3.51	6.85	3.92	3.56	2.67	4.94	3.27	2.35	1.41	2.01	2.65	6.19	3.20
ΣREE	14.3	13.5	21.2	18.9	30.1	45.6	39.2	21.3	46.1	49.6	52.3	74.4	87.0	122	104	97.1	64.2	57.0	52.8	60.6	65.6	96.4	108	83.6
Eu/Eu*	0.88	0.78	0.65	0.68	0.97	0.66	0.75	0.85	0.69	0.88	0.84	0.86	0.46	0.73	0.69	0.72	0.72	0.49	0.80	0.59	0.91	0.85	0.63	0.61
Ce/Ce*	1.22	1.25	1.45	1.65	1.52	1.33	1.22	1.30	2.10	1.62	1.63	1.64	1.37	1.90	1.89	1.13	1.35	1.08	1.69	0.93	1.47	1.35	2.53	2.53

Layer	LB										HS				HS				HL						
	Sample	X-8	W-8	W-9	W-10	W-11	S-6	S-7	Y-6	Y-7	Y-8	W-12	W-13	X-9	X-10	S-8	S-9	Y-9	Y-10	X-11	X-12	X-13	Y-11	W-14	W-15
SiO <sub>2</sub> (wt.%)	26.23	40.42	42.66	43.60	37.39	42.15	43.85	41.53	23.70	33.20	66.16	59.02	62.36	63.30	66.27	57.89	60.73	61.98	2.48	1.62	0.74	0.24	0.55	0.27	
Al <sub>2</sub> O <sub>3</sub>	53.02	35.40	35.25	38.36	31.77	34.71	27.67	30.94	41.59	51.40	14.14	19.89	21.58	18.52	16.52	20.68	16.49	16.31	0.56	0.50	1.73	0.10	0.37	0.12	
TiO <sub>2</sub>	2.04	0.78	1.00	0.75	0.61	1.05	0.38	0.49	1.32	1.52	0.25	0.36	0.42	0.37	0.36	0.27	0.32	0.34	0.05	0.05	0.06	0.03	0.05	0.02	
Fe <sub>2</sub> O <sub>3</sub>	3.78	5.05	4.56	2.10	21.10	6.80	9.20	8.23	14.69	1.48	7.56	7.80	7.16	7.30	5.26	8.12	6.97	7.19	0.32	0.25	0.22	0.21	0.23	0.31	
Na <sub>2</sub> O	0.64	1.72	0.52	0.32	0.33	0.86	0.76	1.05	0.44	0.56	4.53	3.14	0.22	0.34	0.61	0.37	3.54	3.03	0.07	0.32	0.18	0.03	0.06	0.02	
K <sub>2</sub> O	1.46	1.29	0.79	0.21	0.86	4.67	3.97	2.68	0.31	0.32	0.41	0.45	2.31	2.34	2.00	2.80	0.91	0.67	0.05	0.35	0.08	0.18	0.05	0.16	
CaO	0.32	0.70	1.01	0.38	1.59	0.30	0.40	0.40	0.13	0.45	1.85	1.25	0.60	0.46	0.93	0.49	2.25	2.40	54.00	54.60	53.67	55.27	55.27	55.74	
MgO	0.67	1.24	0.55	0.29	0.59	0.92	2.18	1.88	3.82	0.50	1.84	2.48	2.37	2.23	1.85	2.21	3.18	2.80	0.16	0.19	0.13	0.53	0.12	0.33	
MnO	0.01	0.01	0.00	0.04	0.01	0.01	0.03	0.02	0.05	0.02	0.02	0.04	0.05	0.06	0.06	0.04	0.04	0.05	0.01	0.01	0.01	0.20	0.01	0.17	
P <sub>2</sub> O <sub>5</sub>	0.10	0.05	0.04	0.13	0.05	0.13	0.07	0.07	0.10	0.15	0.06	0.04	0.10	0.09	0.13	0.11	0.06	0.06	0.06	0.10	0.03	0.06	0.06	0.03	
LOI	11.62	13.46	13.39	13.66	5.62	8.45	11.35	12.45	13.68	10.47	3.28	5.32	2.69	4.76	5.89	6.93	5.52	5.33	42.36	42.12	42.90	43.09	43.02	42.67	
Total	99.89	100.13	99.77	99.84	99.91	100.05	99.86	99.74	99.83	100.07	100.11	99.80	99.86	99.76	99.88	99.91	99.73	100.16	100.13	100.06	99.82	99.91	99.78	99.84	
Rb (ppm)	77.5	43.2	14.1	28.8	12.2	183	224	161	3.54	111	192	171	180	175	157	217	204	176	14.1	7.05	0.29	0.50	2.19	0.00	
Ba	297	422	92.4	91.8	78.0	315	382	231	66.0	613	327	347	426	438	338	408	420	343	32.2	36.7	5.36	3.56	124	2.26	
Th	38.1	49.1	32.6	28.5	79.3	30.4	32.3	39.7	65.8	61.8	17.7	17.5	17.0	17.0	16.1	18.1	16.7	16.8	1.29	0.63	0.13	0.09	0.50	0.04	
U	11.9	17.63	3.33	4.87	3.82	4.90	9.37	9.33	7.75	12.9	2.83	2.50	2.70	2.80	2.03	2.90	2.42	2.33	15.50	6.38	0.13	0.10	0.17	0.63	
Ta	3.68	4.25	2.65	3.36	2.44	2.51	2.15	2.22	3.99	5.36	1.14	1.12	1.23	1.19	1.16	1.16	1.01	1.09	0.18	0.14	0.07	0.04	0.29	0.01	
Nb	46.5	56.3	34.4	42.2	35.0	35.2	28.6	30.5	53.1	63.8	15.3	14.1	17.2	16.5	15.0	16.0	13.3	14.7	1.23	0.80	0.20	0.11	0.52	0.06	
Sr	168	149	124	116	669	178	248	352	150	226	163	134	63.4	62.9	113	107	85.5	139	165	164	279	138	214	104	
Y	36.7	30.4	29.6	22.9	41.4	32.8	40.6	25.1	46.5	38.2	33.7	26.2	32.2	31.3	30.0	23.0	23.2	29.8	5.15	4.92	10.7	12.4	10.2	15.4	
Zr	464	396	373	454	392	381	236	349	619	659	163	127	160	157	177	131	121	145	8.86	8.37	0.83	1.30	8.39	0.46	
V	305	84	194	159	154	344	284	248	321	279	94	108	119	113	91	126	116	110	39	12.1	3.81	1.70	1.78	8.66	
Cr	191	142	166	163	172	330	258	297	359	393	76	81	95	89	71	95	91	85	6	8.63	6.66	10.3	5.30	10.6	
Ni	60.5	12.5	110	70.3	71.6	161	37.5	13.4	70.4	73.3	43.6	40.5	47.8	45.8	36.8	47.1	50.4	42.5	12.3	17.0	16.6	16.2	10.5	13.3	
Ga	38.0	41.6	30.2	26.4	36.1	31.4	33.2	45.9	87.1	57.5	19.6	21.6	21.4	21.3	17.6	23.7	22.7	22.5	2.17	1.02	0.20	0.23	0.80	0.15	
Hf	12.9	10.8	9.91	12.2	10.6	9.95	6.78	9.68	17.4	18.0	4.29	3.38	4.19	4.12	4.69	3.36	3.18	3.83	0.24	0.18	0.03	0.02	0.25	0.01	
La	88.0	33.6	124	28.5	120	81.4	63.4	35.5	12.8	73.7	44.2	45.6	44.1	44.2	37.8	44.8	45.3	42.4	3.75	3.06	2.48	2.06	4.63	4.80	
Ce	182	93.3	562	68.0	439	121	141	73.4	114	183	87.1	88.0	85.0	86.4	74.1	82.2	87.8	85.3	7.06	3.87	2.06	1.42	4.36	0.66	
Pr	23.3	9.09	24.4	4.02	37.4	16.1	14.5	7.48	3.70	17.8	10.2	9.70	10.0	10.1	8.73	9.12	9.59	9.36	0.86	0.69	0.55	0.45	1.00	0.96	
Nd	79.4	31.5	80.8	10.8	152	50.2	52.6	25.8	13.2	58.9	39.1	34.8	37.3	37.6	33.3	31.7	34.4	34.2	3.34	2.95	2.48	2.26	4.24	4.43	
Sm	13.9	6.55	15.1	2.08	25.0	6.26	10.8	4.84	3.22	9.22	7.63	6.03	7.72	7.69	7.14	5.21	5.65	6.44	0.71	0.64	0.61	0.78	1.10	1.26	
Eu	2.78	1.08	2.37	0.50	4.16	0.99	2.46	1.09	0.92	1.56	1.59	1.16	1.74	1.70	1.53	1.05	1.12	1.25	0.22	0.15	0.24	0.21	0.27	0.30	
Gd	10.6	5.37	10.1	2.94	14.1	4.79	10.5	4.30	5.43	7.35	6.92	4.99	7.56	7.51	6.82	4.57	4.70	5.70	0.77	0.71	0.97	1.25	1.41	1.67	
Tb	1.77	1.02	1.63	0.59	1.81	0.93	1.54	0.75	1.10	1.16	1.07	0.79	1.11	1.11	1.03	0.74	0.71	0.91	0.13	0.10	0.14	0.16	0.22	0.28	
Dy	9.23	6.23	8.88	4.16	8.46	5.66	7.90	4.06	7.58	6.85	5.82	4.50	5.77	5.76	5.56	4.04	4.00	4.91	0.67	0.53	0.81	0.83	1.22	1.92	
Ho	1.91	1.38	1.86	0.92	1.73	1.43	1.59	0.90	1.90	1.54	1.21	1.02	1.21	1.20	1.19	0.89	0.90	1.13	0.15	0.11	0.20	0.18	0.26	0.44	
Er	5.52	3.98	5.77	2.92	4.78	4.55	4.36	2.69	5.47	5.14	3.21	2.72	3.27	3.04	3.11	2.52	2.58	3.01	0.43	0.27	0.51	0.35	0.72	0.95	
Tm	0.80	0.60	1.01	0.44	0.69	0.71	0.61	0.41	0.87	0.83	0.45	0.40	0.44	0.43	0.43	0.37	0.34	0.43	0.06	0.03	0.06	0.03	0.09	0.11	
Yb	5.63	3.96	8.16	3.21	4.71	4.99	4.24	2.94	5.93	6.14	2.80	2.72	3.04	2.95	2.85	2.47	2.52	2.84	0.36	0.22	0.37	0.20	0.56	0.61	
Lu	0.80	0.59	1.22	0.47	0.66	0.78	0.63	0.43	0.93	0.93	0.40	0.38	0.45	0.43	0.42	0.37	0.37	0.39	0.05	0.03	0.06	0.02	0.08	0.08	
ΣLREE	387	174	806	113	773	275	282	147	147	343	188	184	184	186	161	173	183	178	15.7	11.2	8.18	6.98	15.3	12.1	
ΣHREE	39.1	24.2	41.0	16.2	41.1	24.8	33.8	17.6	30.1	31.5	23.5	18.7	24.6	24.2	22.9	17.0	17.2	20.6	2.83	2.15	3.36	3.24	4.84	6.36	
ΣLREE/ΣHREE	9.89	7.19	19.7	7.02	18.8	11.1	8.35	8.37	4.88	10.9	8.02	9.86	7.49	7.70	7.02	10.2	10.6	8.64	5.55	5.22	2.43	2.16	3.16	1.90	
ΣREE	426	198	847	130	814	300	316	165	177	374	212	203	209	210	184	190	200	198	18.6	13.4	11.5	10.2	20.2	18.5	
Eu/Eu*	0.67	0.54	0.55	0.62	0.62	0.53	0.70	0.72	0.67	0.56	0.66	0.63	0.69	0.68	0.66	0.64	0.64	0.62	0.89	0.67	0.95	0.65	0.67	0.64	
Ce/Ce*	0.96	1.28	2.35	1.37	1.60	0.77	1.10	1.05	4.01	1.20	0.97	0.98	0.95	0.96	0.96	0.94	0.98	1.01	0.93	0.63	0.42	0.34	0.47	0.07	

ΣREE = ΣLREE (La–Lu), ΣLREE = ΣLREE (La–Eu) and ΣHREE = ΣLREE (Gd–Lu). Eu/Eu\* = (2Eu / Eu<sub>ch</sub>) / (Sm/Sm<sub>ch</sub> + Gd / Gd<sub>ch</sub>), Ce/Ce\* = (2Ce / Ce<sub>ch</sub>) / (La / La<sub>ch</sub> + Pr / Pr<sub>ch</sub>).

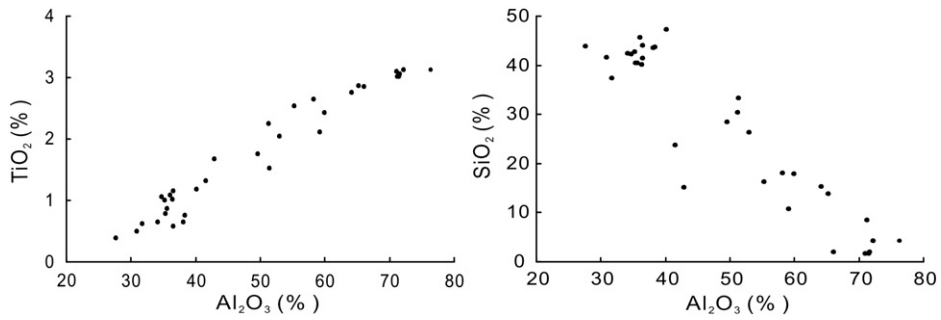


Fig. 8. Binary diagrams of average TiO<sub>2</sub> (wt.%) and average SiO<sub>2</sub> (wt.%) against average Al<sub>2</sub>O<sub>3</sub> contents (wt.%) of the bauxites.

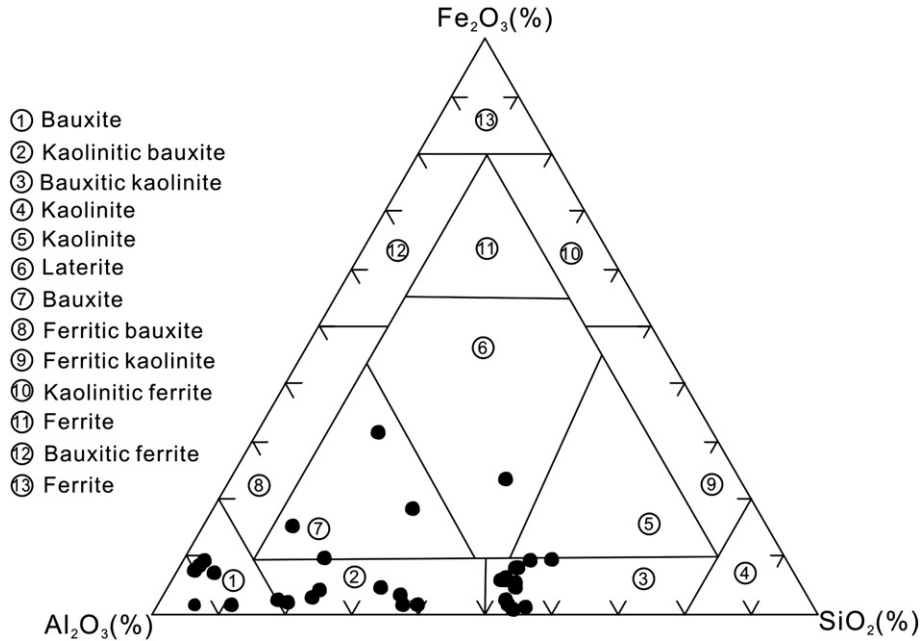


Fig. 9. The Fe<sub>2</sub>O<sub>3</sub>-Al<sub>2</sub>O<sub>3</sub>-SiO<sub>2</sub> triangular diagram showing the mineralogical classification of the bauxite ores in the WZD area (after Aleva, 1994).

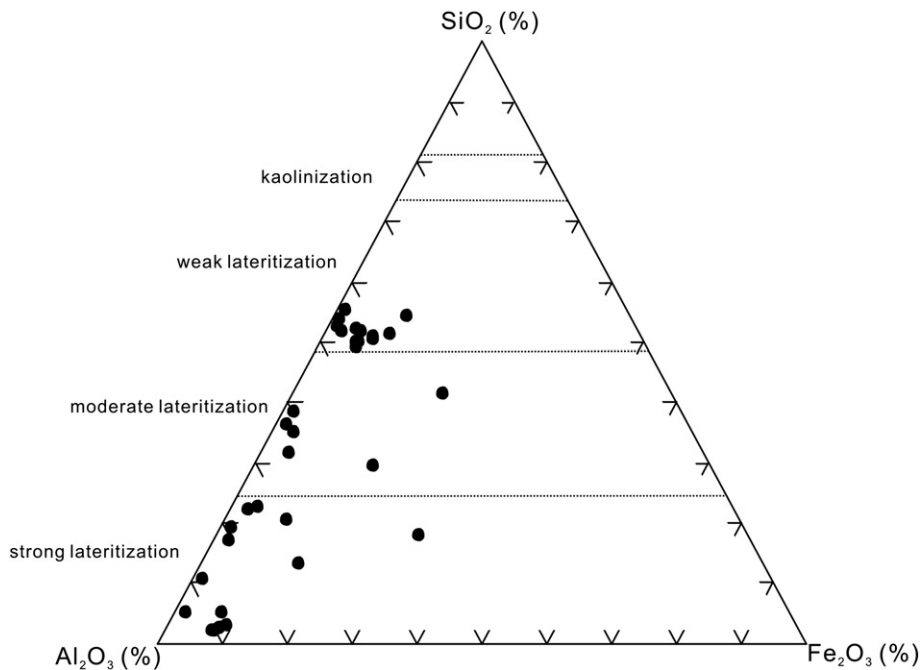


Fig. 10. The Al<sub>2</sub>O<sub>3</sub>-SiO<sub>2</sub>-Fe<sub>2</sub>O<sub>3</sub> triangular diagram of bauxites showing degree of lateritization (after Schellmann, 1982).

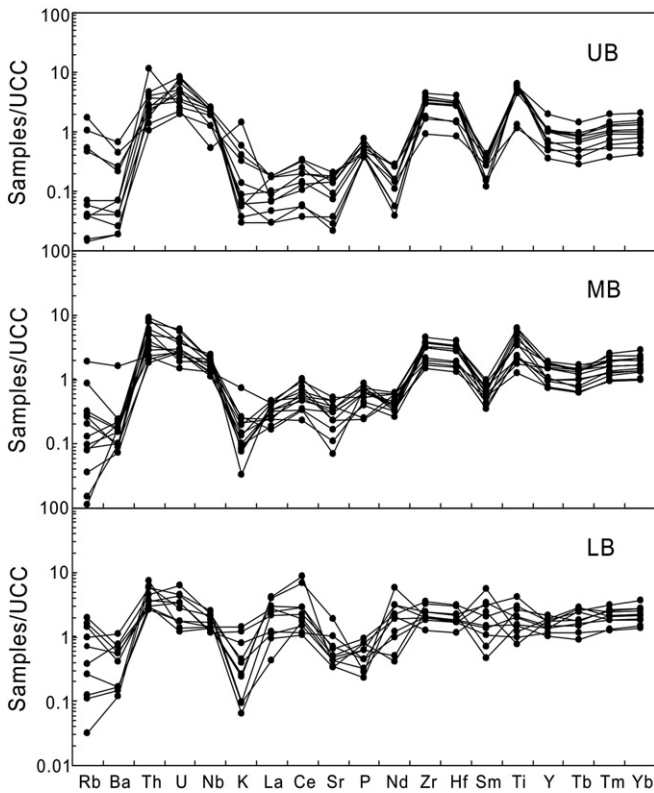


Fig. 11. UCC-normalized trace element spidergrams of the bauxites from different horizons of the bauxite deposits in the study area, normalizing values from Taylor and McLennan (1985).

not be precluded. REEs are negatively correlated to Al (Table 3), which suggest REE contents generally decrease with increased bauxitization. Such a trend is also described from other lateritic bauxite deposit (Boulange et al., 1990).

Basic properties of the REE, pH precipitation of their hydroxides, markedly decrease from La to Lu (from pH 8.4 to 6.0) (Karadag et al., 2009). Therefore, the pH is a very important factor for the fractionation of REE in the sedimentary cycle (Nesbitt, 1979). Under acidic conditions, REEs are easily removed from weathering products, but they are fixed by major scavengers under neutral to alkaline

conditions (Karadag et al., 2009; Nesbitt, 1979). In connection with this, a progressive enrichment of the REE towards the bottom of the deposits in the WZD region is well pronounced. We can expect, therefore, that in a ground-surface environment, where the waters are acidic, the trivalent rare earth element ions cannot easily be absorbed in clay minerals and mostly migrate downward with the solutions. In comparison, a lack of active drainage in the lower bauxitic clay and the nature of its interface with carbonate rocks are the main reasons for the dominance of weakly alkaline to alkaline pH values, leading to REE concentration in the lowermost horizon. This also explains the weak bauxitization observed in the lower horizon and the evolution of the bauxitic clay.

Moreover, there is a strong connection between REE ionic potential and their mobility (Esmaily et al., 2010). This is consistent with the distribution pattern of REE in the WZD bauxite deposits. Most of the bauxite samples show positive Ce anomalies, while few samples in the lower bauxitic layer show negative Ce anomaly. Ce exists naturally in two forms:  $Ce^{3+}$  and  $Ce^{4+}$ , with  $Ce^{4+}$  having a higher ionic potential than the other LREE and consequently the lowest mobility (Esmaily et al., 2010). Accordingly, Ce is usually retained in the upper parts of the weathering profiles due to the oxidation of  $Ce^{3+}$  to  $Ce^{4+}$  (Compton et al., 2003; Karadag et al., 2009; Nyakairu et al., 2001). The lower ionic potential of LREE relative to HREE means that they were readily leached from the upper layers and concentrated in the lowermost section. In contrast, the high ionic potential of  $Ce^{4+}$  means that it behaved as a HREE, and was concentrated in the upper layers.

To summarize, carrier minerals contained in the bauxite, pH variations in weathering solutions, adsorption process, groundwater chemical characteristics, Fe concentration variations in weathering profiles, leaching degree of minerals and geochemistry characteristics of elements (solubility, ionic potential, pH of hydroxide precipitation, cation exchange capacity, exchangeable cations, and possibility of complex formation) have been shown to play vital role in distribution of trace and rare earth elements during weathering of the lateritic bauxite in the WZD area.

### 5.3. Ore-forming process

According to the data obtained in this study, we can conclude that the WZD bauxites were likely derived from the Hanjiadian mud shale and argillic phase within the Huanglong limestone with the precursors of them most likely the Neoproterozoic basic igneous rocks and the

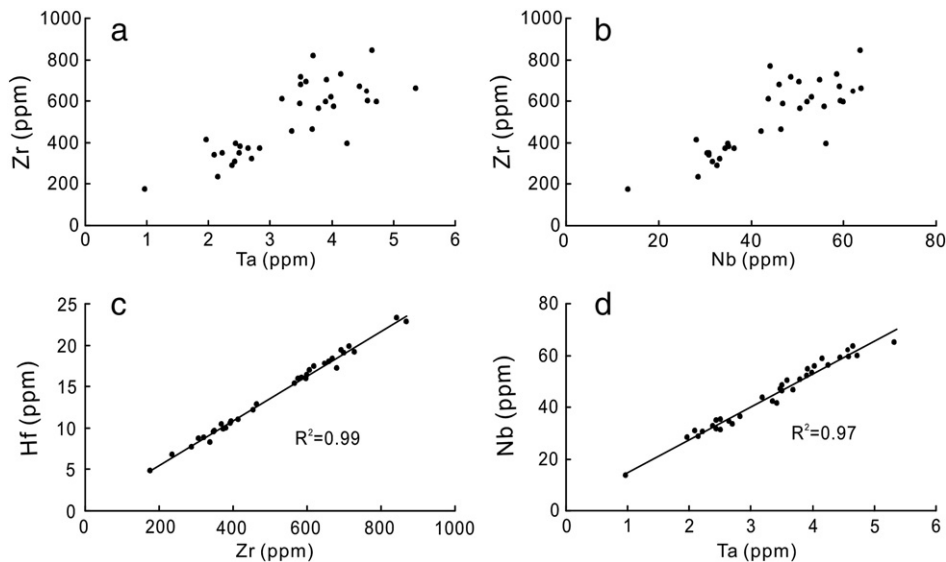


Fig. 12. Binary diagrams showing the correlations between a) Zr and Ta; b) Zr and Nb; c) Hf and Zr; and d) Nb and Ta for the bauxites in the study area.

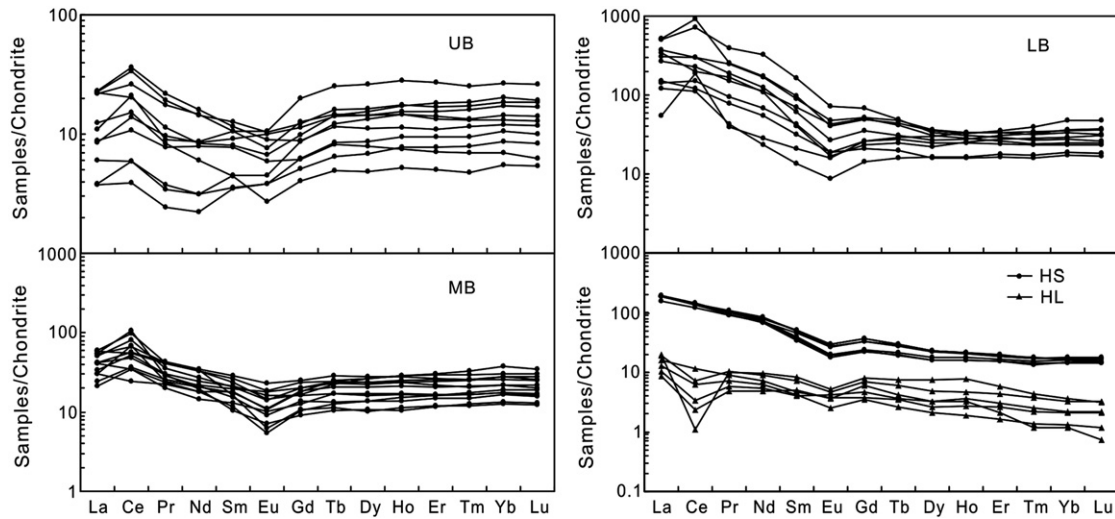


Fig. 13. Chondrite-normalized REE patterns of the bauxites (UB, MB, LB), Hanjiadian mud shale (HS) and Huanglong limestone (HL), normalizing values from Sun and McDonough (1989).

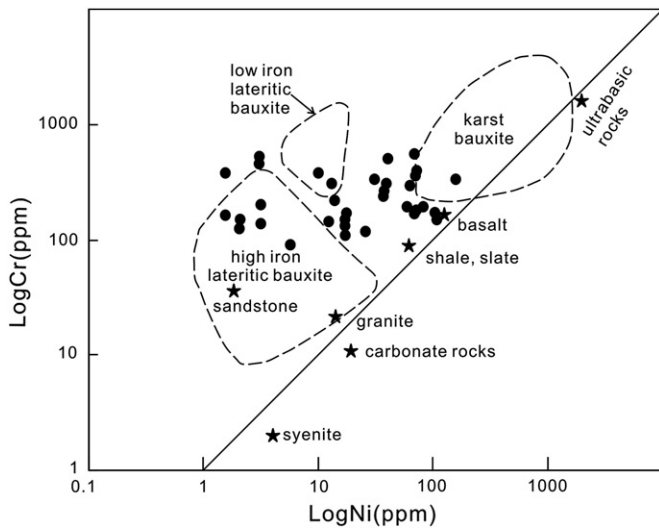


Fig. 14. Plot of Ni versus Cr concentration values for various types of bauxites in relation to various precursor rocks (after Schroll and Sauer, 1968).

Mesoproterozoic basic-ultrabasic intrusions in the southern Yangtze Block. Based on the mineralogical, petrographical and geochemical analyzes, the following ore forming processes are proposed:

Stage 1: Primary minerals (feldspar, ferromagnesians, heavy minerals, etc.) of the basic rocks were weathered to kaolinite, sericite, quartz, and small amounts of calcite, chlorite, hematite, goethite,

rutile, anatase and amorphous materials. During this stage, immobile elements such as Al, Fe, Ti, Cr, Nb, Ga, Ta, Hf and REEs should have been slightly enriched while alkalis were leached from the system. During Cambrian to Middle Silurian times, the region experienced a large transgression–regression cycle under the influence of the first stage of Caledonian movement, which resulted in the deposition of weakly weathered materials mentioned above in the Paleotethys Ocean to form Cambro-Ordovician carbonate rocks and the Hanjiadian mud shale.

Stage 2: During Upper Silurian to Upper Carboniferous, a fall in sea level led to an epeirogenic phase and the subaerial exposure of the Hanjiadian Group while sedimentation ceased. At the same time, the Hanjiadian mud shale rich in aluminum and iron were subjected to lateritic weathering under subtropic–tropical climate conditions, forming a thick paleo-weathering crust. During the early stage of the lateritic weathering, alkalis were leached from the system by acidic solutions, while insoluble elements such as Al, Ti, Fe and Si were reprecipitated as simple oxides, resulting in the accumulation of bauxitic materials, Fe and Ti oxides, and clay minerals which are phases that host bauxite.

Stage 3: At the latest Carboniferous, the Huanglong limestone was discontinuously deposited only in the depressions of the Hanjiadian Group. Field observations, mineralogical and geochemical data suggest that Huanglong limestone could be supplied by the Hanjiadian mud shale. In the following transgression at the beginning of Middle Permian, the weathered bauxitic materials were transported for a short distance and finally deposited on the depressions of Silurian Hanjiadian Group, or on the limestone erosion surface of the Upper Carboniferous Huanglong Formation. The weathered bauxitic materials were partly converted to bauxite by means of progressive

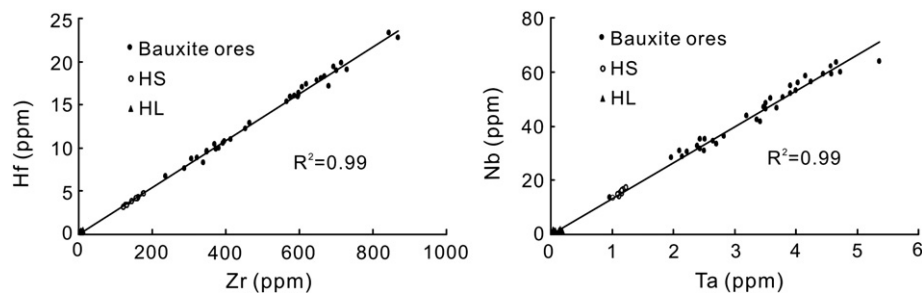


Fig. 15. Binary diagrams showing the correlations between Zr and Ta; Zr and Nb for the bauxite ores, Hanjiadian mud shale (HS) and Huanglong limestone (HL).

**Table 3**

Correlation coefficients of major oxides and REEs of the bauxites from the study area.

	SiO <sub>2</sub>	Al <sub>2</sub> O <sub>3</sub>	TiO <sub>2</sub>	Fe <sub>2</sub> O <sub>3</sub>	Na <sub>2</sub> O	K <sub>2</sub> O	CaO	MgO	MnO	P <sub>2</sub> O <sub>5</sub>
La	0.41	−0.45	−0.43	0.25	−0.18	0.28	0.59	−0.14	−0.16	−0.11
Ce	0.34	−0.40	−0.38	0.31	−0.19	0.09	0.66	−0.09	−0.13	−0.24
Pr	0.35	−0.41	−0.40	0.34	−0.17	0.22	0.65	−0.13	−0.14	−0.14
Nd	0.32	−0.39	−0.38	0.39	−0.17	0.19	0.69	−0.12	−0.13	−0.18
Sm	0.29	−0.38	−0.37	0.41	−0.14	0.16	0.69	−0.07	−0.10	−0.23
Eu	0.19	−0.31	−0.29	0.46	−0.09	0.16	0.61	0.01	−0.02	−0.20
Gd	0.20	−0.34	−0.32	0.47	−0.10	0.16	0.55	0.11	0.03	−0.15
Tb	0.11	−0.26	−0.22	0.45	−0.02	0.13	0.46	0.21	0.12	−0.13
Dy	0.01	−0.18	−0.12	0.43	0.04	0.05	0.37	0.30	0.22	−0.07
Ho	0.03	−0.15	−0.08	0.44	0.06	0.02	0.31	0.36	0.25	−0.04
Er	0.03	−0.20	−0.12	0.41	0.04	0.03	0.32	0.31	0.21	0.01
Tm	0.06	−0.21	−0.13	0.37	0.02	0.00	0.34	0.27	0.16	−0.02
Yb	0.10	−0.23	−0.15	0.33	−0.02	−0.01	0.37	0.22	0.12	−0.04
Lu	0.10	−0.24	−0.16	0.33	0.00	0.00	0.33	0.25	0.13	−0.01
ΣREE	0.35	−0.42	−0.40	0.34	−0.18	0.15	0.67	−0.09	−0.13	−0.21

in situ lateritic weathering. The warm humid climate condition and a dense forest cover led to the formation of lateritic bauxite at that time. During this stage, large amounts of alkalis and silica were leached from the system, while less mobile or immobile elements such as Al, Fe, Ti, Cr and REEs were retained in the different layers of the lateritic profiles. The main aluminum minerals of the bauxite ores formed at this stage are gibbsite and boehmite.

Stage 4: Bauxitic–lateritic horizons were subsequently preserved by deposition of limestone of the Qixia and Maokou Formations and other sediments. Subsidence followed, the bauxite underwent diagenesis, low-grade metamorphism and the thermal overprint from the eruption of the Emeishan flood basalts (e.g., Xu et al., 2001), leading to the formation of diasporite by the dehydration of gibbsite. Folding and faulting at the end of the late Triassic, with ensuing erosion, exposed the bauxitic–lateritic horizons on the limbs of synclines. Bauxite ores subjected to lateritic weathering again, resulting in the formation of high-grade bauxite deposit by further desilication, deferrization and desulfuration. Some kaolinite formed at this stage via epigenetic replacement of alumina in diasporite by dissolved silica.

## 6. Conclusion

The main conclusions from this study are summarized below.

- (1) Mineralogical analyses reveal that diasporite, boehmite, kaolinite, smectite, illite and hematite are the major mineral components in the bauxite ores; gibbsite, chlorite, pyrophyllite, goethite, pyrite and anatase are minor minerals and other minerals such as zircon, rutile, calcite, quartz, feldspar, limonite, dolomite and calcite occur as accessories. During the formation of Wuchuan–Zhengan–Daozhen bauxites, Al-enriched solutions precipitated gibbsite and boehmite firstly, and later low-grade metamorphism and the thermal action under the influence of the eruption of the Emeishan flood basalts, lead to the formation of diasporite by the dehydration of gibbsite. The textural features of ores suggest that the bauxite has an authigenic origin but locally experienced transportation and re-deposition.
- (2) The main components of the ores are Al<sub>2</sub>O<sub>3</sub>, Fe<sub>2</sub>O<sub>3</sub>, SiO<sub>2</sub> and TiO<sub>2</sub>. Immobile elements like Zr, Cr, Hf, Nb, Ta, Th, U and REEs were distinctly enriched during the bauxitization. Factors such as carrier minerals contained in the bauxite, pH variations in weathering solutions, adsorption process, groundwater chemical characteristics, Fe concentration variations in weathering profiles, leaching degree of minerals and geochemical characteristics of elements have been shown to play vital role in

distribution of trace and rare earth elements during weathering of the lateritic bauxite.

- (3) Geochemical characteristics suggested that the bauxite deposits were derived from Hanjiadian mud shales and argillite sections within Huanglong limestone. Furthermore, buried Precambrian rocks of basic precursors, probably the Neoproterozoic basic igneous rocks and the Mesoproterozoic basic–ultrabasic intrusions in the Yangtze Block, could have been the main source of the Hanjiadian Formation.

## Acknowledgment

We appreciate the assistances of S.S. Peng in major element analyses, J. Hu, G.P. Bao and Y. Huang for trace element analyses, G.H. Gong for XRD analyses, W.Q. Zheng and S.R. Liu for SEM analyses. The paper has benefited from review comments of two anonymous referees. This work is jointly supported by the Key Research Program of the Chinese Academy of Sciences (KZCX2-YW-Q04-05) and a Special Research Fund of the SKLOG, IGCAS (KCZX20090103).

## References

- Aleva, G.J.J., 1994. Laterites: Concepts, Geology, Morphology and Chemistry. International Soil Reference and Information Centre, Wageningen, the Netherlands (169 pp.).
- Andrews, J.E., Greenaway, A.M., Dennis, P.F., Barnes-Leslie, D.A., 2001. Isotopic effects on inorganic carbon in a tropical river caused by caustic discharges from bauxite processing. *Applied Geochemistry* 16, 197–206.
- Bárdossy, G., 1982. Karst bauxites, bauxite deposits on carbonate rocks. *Developments in Economic Geology* 14, 1–441.
- Bárdossy, G., Aleva, G.J.J., 1990. Lateritic bauxites. *Developments in Economic Geology*, 27. Elsevier, Amsterdam.
- Bárdossy, G., Kovács, Ó., 1995. A multivariate statistical and geostatistical study on the geochemistry of allochthonous karst bauxite deposits in Hungary. *Natural Resources Research* 4, 138–153.
- BGMRCX (Bureau of Geology and Mineral Resources of Guangxi province), 1985. Regional Geology of Guangxi Autonomous Region. Geological Publishing House, Beijing 1–853 (in Chinese with English abstract).
- Boulange, B., Muller, J.P., Sigolo, J.B., 1990. Behaviour of the rare earth elements in a lateritic bauxite from syenite (Bresil). *Geochemistry of the Earth's Surface and of Mineral Formation*, 2 350–351.
- Boulange, B., Bouzat, G., Pouliquen, M., 1996. Mineralogical and geochemical characteristics of two bauxitic profiles, Fria, Guinea Republic. *Mineralium Deposita* 31, 432–438.
- Braun, J.J., Pagel, M., Herbillon, A., Rosin, C., 1993. Mobilization and redistribution of REEs and thorium in a syenitic lateritic profile: a mass balance study. *Geochimica et Cosmochimica Acta* 57, 4419–4434.
- Calagari, A.A., Abedini, A., 2007. Geochemical investigations on Permo-Triassic bauxite horizon at Kanisheeteh, east of Bukan, West-Azarbaidjan, Iran. *Journal of Geochemical Exploration* 94, 1–18.
- Chen, Q., Zeng, W., Chen, X., Gu, S., Yang, G., Zhou, H., Yin, Z., 1995. Investigation of the thermodynamic properties of  $\gamma$ -Al<sub>2</sub>O<sub>3</sub>. *Thermochemica Acta* 253, 33–39.
- Compton, J.S., White, R.A., Smith, M., 2003. Rare earth element behavior in soils and salt pan sediments of a semi-arid granitic terrain in the Western Cape, South Africa. *Chemical Geology* 201, 239–255.

- Condie, K.C., 1991. Another look at rare-earth elements in shales. *Geochimica et Cosmochimica Acta* 55, 2527–2531.
- Esmaily, D., Rahimpour-Bonab, H., Esna-Ashari, A., Kananian, A., 2010. Petrography and geochemistry of the Jajarm Karst bauxite ore deposit, NE Iran: implications for source rock material and ore genesis. *Turkish Journal of Earth Sciences* 19, 267–284.
- Fan, H.P., Zhu, W.G., Li, Z.X., Zhong, H., Bai, Z.J., He, D.F., Chen, C.J., Cao, C.Y., 2013. Ca. 1.5 Ga mafic magmatism in South China during the break-up of the supercontinent Nuna/Columbia: the Zhuqing Fe–Ti–V oxide ore-bearing mafic intrusions in western Yangtze Block. *Lithos*. <http://dx.doi.org/10.1016/j.lithos.2013.02.004>.
- Galan, E., Fernandez-Caliani, J.C., Miras, A., Aparicio, P., Marquez, M.G., 2007. Residence and fractionation of rare earth elements during kaolinization of alkaline peraluminous granites in NW Spain. *Clay Minerals* 42, 341–352.
- Grubb, P.L.C., 1963. Critical factors in the genesis, extent and grade of some residual bauxite deposits. *Economic Geology* 58, 1267–1277.
- GXRGS (Guangxi Regional Geological Survey Team), 1987. Regional Geological Survey Report (Baotan area, 1:50000), 1–294 (in Chinese).
- GXRGS (Guangxi Regional Geological Survey Team), 1995. Regional Geological Survey Report (Sanfang area, 1:50000), 1–225 (in Chinese).
- GZBGM (Guizhou Bureau of Geology and Mineral Resources), 1987. Regional Geology of Guizhou Province. Geological Publishing House, Beijing 1–704 (in Chinese with English abstract).
- Hill, I.G., Worden, R.H., Meighan, I.G., 2000. Geochemical evolution of a palaeolaterite: the Interbasaltic Formation, Northern Ireland. *Chemical Geology* 166, 65–84.
- Horbe, A.M.C., da Costa, M.L., 1999. Geochemical evolution of a lateritic Sn–Zr–Th–Nb–Y–REE-bearing ore body derived from apogranite: the case of Pitinga, Amazonas – Brazil. *Journal of Geochemical Exploration* 66, 339–351.
- Jiao, W.F., Wu, Y.B., Yang, S.H., Peng, M., Wang, J., 2009. The oldest basement rock in the Yangtze Craton revealed by zircon U–Pb age and Hf isotope composition. *Science in China Series D: Earth Sciences* 52, 1393–1399.
- Jin, Z.G., Wu, G.H., Huang, Z.L., Bao, M., Zhou, J.X., 2009. The geochemical characteristics of Wuchangping bauxite deposit in Wuchuan County, Guizhou Province, China. *Acta Mineralogica Sinica* 29, 458–462 (in Chinese with English abstract).
- Karadag, M.M., Kupeli, S., Aryk, F., Ayhan, A., Zedef, V., Doyen, A., 2009. Rare earth element (REE) geochemistry and genetic implications of the Mortas bauxite deposit (Seydisehir/Konya – Southern Turkey). *Chemie Der Erde – Geochemistry* 69, 143–159.
- Klopprogge, J.T., Ruan, H.D., Frost, R.L., 2002. Thermal decomposition of bauxite minerals: infrared emission spectroscopy of gibbsite, boehmite and diasporite. *Journal of Materials Science* 37, 1121–1129.
- Koppi, A.J., Edis, R., Field, D.J., Geering, H.R., Klessa, D.A., Cockayne, D.J.H., 1996. Rare earth element trends and cerium–uranium–manganese associations in weathered rock from Koongarra, northern territory, Australia. *Geochimica et Cosmochimica Acta* 60, 1695–1707.
- Kühnel, R.A., 1987. The role of cationic and anionic scavengers in laterites. *Chemical Geology* 60, 31–40.
- Laufer, F., Yariv, S., Steinberg, M., 1984. The adsorption of quadrivalent cerium by kaolinite. *Clay Minerals* 19, 137–149.
- Li, X.H., McCulloch, M.T., 1996. Secular variation in the Nd isotopic composition of Neoproterozoic sediments from the southern margin of the Yangtze Block: evidence for a Proterozoic continental collision in southeast China. *Precambrian Research* 76, 67–76.
- Li, X.H., Li, Z.X., Zhou, H., Liu, Y., Kinny, P.D., 2002. U–Pb zircon geochronology, geochemistry and Nd isotopic study of Neoproterozoic bimodal volcanic rocks in the Kangdian Rift of South China: implications for the initial rifting of Rodinia. *Precambrian Research* 113, 135–154.
- Li, X.H., Li, W.X., Li, Z.X., Lo, C.H., Wang, J., Ye, M.F., Yang, Y.H., 2009. Amalgamation between the Yangtze and Cathaysia Blocks in South China: constraints from SHRIMP U–Pb zircon ages, geochemistry and Nd–Hf isotopes of the Shuangxiwu volcanic rocks. *Precambrian Research* 174, 117–128.
- Liaghat, S., Hosseini, M., Zarasvandi, A., 2003. Determination of the origin and mass change geochemistry during bauxitization process at the Hangam deposit, SW Iran. *Geochimical Journal* 37, 627–637.
- Liu, P., 2007. Bauxite geology in the Wuchuan–Zhengan–Daozhen area, Northern Guizhou. *Geology and Prospecting* 43, 29–33 (in Chinese with English abstract).
- Liu, X., Wang, Q., Deng, J., Zhang, Q., Sun, S., Meng, J., 2010a. Mineralogical and geochemical investigations of the Dajia Salento-type bauxite deposits, western Guangxi, China. *Journal of Geochemical Exploration* 105, 137–152.
- Liu, Y., Xia, Y., Wang, J., 2010b. Metallogenic characteristics and metallogenic factors of bauxite deposits in Northern Guizhou. *Bulletin of Mineralogy, Petrology and Geochemistry* 29, 422–425 (in Chinese with English abstract).
- Liu, X., Wang, Q., Zhang, Q., Feng, Y., Cai, S., 2012. Mineralogical characteristics of the superlarge quaternary bauxite deposits in Jingxi and Debao counties, western Guangxi, China. *Journal of Asian Earth Sciences* 52, 53–62.
- Maclean, W.H., 1990. Mass change calculations in altered rock series. *Mineralium Deposita* 25, 44–49.
- Maclean, W.H., Barrett, T.J., 1993. Litho-geochemical techniques using immobile elements. *Journal of Geochemical Exploration* 48, 109–133.
- Maclean, W.H., Kranidiotis, P., 1987. Immobile elements as monitors of mass transfer in hydrothermal alteration; Phelps Dodge massive sulfide deposit, Matagami, Quebec. *Economic Geology* 82, 951–962.
- Maclean, W.H., Bonavia, F.F., Sanna, G., 1997. Argillite debris converted to bauxite during karst weathering: evidence from immobile element geochemistry at the Olmedo Deposit, Sardinia. *Mineralium Deposita* 32, 607–616.
- Mameli, P., Mongelli, G., Oggiano, G., Dinelli, E., 2007. Geological, geochemical and mineralogical features of some bauxite deposits from Nurra (Western Sardinia, Italy): insights on conditions of formation and parental affinity. *International Journal of Earth Sciences* 96, 887–902.
- Meshram, R.R., Randive, K.R., 2011. Geochemical study of laterites of the Jamnagar district, Gujarat, India: implications on parent rock, mineralogy and tectonics. *Journal of Asian Earth Sciences* 42, 1271–1287.
- Meyer, F.M., Happel, U., Hausberg, J., Wiechowski, A., 2002. The geometry and anatomy of the Los Pijiguao bauxite deposit, Venezuela. *Ore Geology Reviews* 20, 27–54.
- Mongelli, G., 1997. Ce-anomalies in the texture components of Upper Cretaceous karst bauxites from the Apulian carbonate platform (southern Italy). *Chemical Geology* 14, 69–79.
- Mordberg, L.E., 1993. Patterns of distribution and behaviour of trace elements in bauxite. *Chemical Geology* 107, 241–244.
- Mordberg, L.E., Nesterova, E.N., 1996. Palaeozoic bauxite deposits of North Onega basin, Russia: evidence as to genesis. *Transactions of the Institution of Mining and Metallurgy Section B–Applied Earth Science* 105, B200–B205.
- Mordberg, L.E., Spratt, J., 1998. Alteration of zircons: the evidence of Zr mobility during bauxitic weathering. *Goldschmidt Conference Toulouse*, pp. 1021–1022.
- Mutakya, M.K.D., Ikingura, J.R., Mruma, A.H., 2003. Geology and geochemistry of bauxite deposits in Lushoto District, Usambara Mountains, Tanzania. *Journal of African Earth Sciences* 36, 357–369.
- Nesbitt, H.W., 1979. Mobility and fractionation of rare earth elements during weathering of a granodiorite. *Nature* 279, 206–210.
- Nyakairu, G.W.A., Koerber, C., Kurzweil, H., 2001. The Buwambo kaolin deposit in central Uganda: mineralogical and chemical composition. *Geochemical Journal* 35, 245–256.
- Panahi, A., Young, G.M., Rainbird, R.H., 2000. Behavior of major and trace elements (including REE) during Paleoproterozoic pedogenesis and diagenetic alteration of an Archean granite near Ville Marie, Quebec, Canada. *Geochimica et Cosmochimica Acta* 64, 2199–2220.
- Peryea, F.J., Kittrick, J.A., 1988. Relative solubility of corundum, gibbsite, boehmite, and diasporite at standard state conditions. *Clays and Clay Minerals* 36, 391–396.
- Pokrovsky, O.S., Schott, J., Dupre, B., 2006. Trace element fractionation and transport in boreal rivers and soil porewaters of permafrost-dominated basaltic terrain in Central Siberia. *Geochimica et Cosmochimica Acta* 70, 3239–3260.
- Price, G.D., Valdes, P.J., Sellwood, B.W., 1997. Prediction of modern bauxite occurrence: implications for climate reconstruction. *Palaeogeography Palaeoclimatology Palaeoecology* 131, 1–13.
- Qi, L., Hu, J., Grégoire, D.C., 2000. Determination of trace elements in granites by inductively coupled plasma mass spectrometry. *Talanta* 51, 507–513.
- Qiu, Y.M., Gao, S., McNaughton, N.J., Groves, D.L., Ling, W., 2000. First evidence of > 3.2 Ga continental crust in the Yangtze Craton of south China and its implications for Archean crustal evolution and Phanerozoic tectonics. *Geology* 28, 11–14.
- Roaldset, E., 1979. Rare earth elements in different size fractions of a marine quick clay from Ullensaker, and a till from upper Numedal, Norway. *Clay Minerals* 14, 229–240.
- Schellmann, W., 1982. Eine neue Lateritdefinition. *Geologisches Jahrbuch – Reihe D* 58, 31–47.
- Schroll, E., Sauer, D., 1968. Beitrag zur Geochemie von Titan, Chrom, Nickel, Cobalt, Vanadium und Molybdän in bauxitischen Gesteinen und das Problem der stofflichen Herkunft des Aluminiums. *Travaux du ICSOBA*, 5 83–96.
- Sun, S.S., McDonough, W.F., 1989. Chemical and Isotopic Systematics of Oceanic Basalts: Implications for Mantle Composition and Processes. Geological Society, London, Special Publications, 42, pp. 313–345.
- Taylor, S.R., McLennan, S.M., 1985. The Continental Crust: Its Composition and Evolution. Blackwell, London (312 pp.).
- Taylor, G., Eggleton, R.A., Foster, L.D., Tilley, D.B., Le Gleuher, M., Morgan, C.M., 2008. Nature of the Weipa Bauxite deposit, northern Australia. *Australian Journal of Earth Sciences* 55, S45–S70.
- Temur, S., 2006. A geochemical approach to parent rocks of the Maşatdağı diasporic bauxite, Alanya, Antalya, southern Turkey. *Geochemistry International* 44, 941–952.
- Villaseca, C., Romera, C.M., De la Rosa, J., Barbero, L., 2003. Residence and redistribution of REE, Y, Zr, Th and U during granulite-facies metamorphism: behaviour of accessory and major phases in peraluminous granulites of central Spain. *Chemical Geology* 200, 293–323.
- Wang, X.L., Zhou, J.C., Qiu, J.S., Zhang, W.L., Liu, X.M., Zhang, G.L., 2006. LA-ICP-MS U–Pb zircon geochronology of the Neoproterozoic igneous rocks from Northern Guangxi, South China: implications for tectonic evolution. *Precambrian Research* 145, 111–130.
- Wang, Q.F., Deng, J., Liu, X.F., Zhang, Q.Z., Sun, S.L., Jiang, C.Z., Zhou, F., 2010. Discovery of the REE minerals and its geological significance in the Quyang bauxite deposit, West Guangxi, China. *Journal of Asian Earth Sciences* 39, 701–712.
- Wang, Q.F., Liu, X.F., Yan, C.H., Cai, S.H., Li, Z.M., Wang, Y.R., Zhao, J.M., Li, G.J., 2012a. Mineralogical and geochemical studies of boron-rich bauxite ore deposits in the Songqi region, SW Henan, China. *Ore Geology Reviews* 48, 258–270.
- Wang, W., Chen, F.K., Hu, R., Chu, Y., Yang, Y.Z., 2012b. Provenance and tectonic setting of Neoproterozoic sedimentary sequences in the South China Block: evidence from detrital zircon ages and Hf–Nd isotopes. *International Journal of Earth Sciences* 101, 1723–1744.
- Wu, G.H., Liu, Y.P., Zhang, Y.W., 2006. Geological characters and aluminum ore resources potential in the WuChuan–Zhengan–Daozhen area, Guizhou. *Geology and Prospecting* 42, 39–43 (in Chinese with English abstract).
- Wu, G., Jin, Z., Bao, M., Mao, Z., 2008. Bauxite metallogenic regularity in the Wuchuan–Zhengan–Daozhen area, Northern Guizhou. *Geology and Prospecting* 44, 31–35 (in Chinese with English abstract).
- Xu, Y.G., Chung, S.L., Jahn, B.M., Wu, G.Y., 2001. Petrologic and geochemical constraints on the petrogenesis of Permian–Triassic Emeishan flood basalts in southwestern China. *Lithos* 58, 145–168.
- Yan, M., Liu, Y.J., Ma, D.S., 1995. Stratigraphic geochemistry of Upper–Middle Proterozoic Suberathem in northern Guangxi, China. *Chinese Journal of Geochemistry* 14, 231–242.

- Yin, X.H., 2009. Mineralization and metallogenic model for bauxite in the Wuchuan–Zhenan–Daozhen Areas, Northern Guizhou. *Acta Sedimentologica Sinica* 27, 452–457 (in Chinese with English abstract).
- Zarasvandi, A., Charchi, A., Carranza, E.J.M., Alizadeh, B., 2008. Karst bauxite deposits in the Zagros Mountain Belt, Iran. *Ore Geology Reviews* 34, 521–532.
- Zarasvandi, A., Zamanian, H., Hejazi, E., 2010. Immobile elements and mass changes geochemistry at Sar-Faryab bauxite deposit, Zagros Mountains, Iran. *Journal of Geochemical Exploration* 107, 77–85.
- Zhang, S.B., Zheng, Y.F., Wu, Y.B., Zhao, Z.F., Gao, S., Wu, F.Y., 2006. Zircon isotope evidence for  $\geq 3.5$  Ga continental crust in the Yangtze Craton of China. *Precambrian Research* 146, 16–34.
- Zheng, Y.F., Wu, R.X., Wu, Y.B., Zhang, S.B., Yuan, H., Wu, F.Y., 2008. Rift melting of juvenile arc-derived crust: geochemical evidence from Neoproterozoic volcanic and granitic rocks in the Jiangnan Orogen, South China. *Precambrian Research* 163, 351–383.
- Zhou, M.F., Yan, D.P., Kennedy, A.K., Li, Y., Ding, J., 2002. SHRIMP U–Pb zircon geochronological and geochemical evidence for Neoproterozoic arc-magmatism along the western margin of the Yangtze Block, South China. *Earth and Planetary Science Letters* 196, 51–67.
- Zhou, J.C., Wang, X.L., Qiu, J.S., Gao, J.F., 2004. Geochemistry of Meso- and Neoproterozoic mafic–ultramafic rocks from northern Guangxi, China: arc or plume magmatism? *Geochemical Journal* 38, 139–152.
- Zhou, J.C., Wang, X.L., Qiu, J.S., 2009. Geochronology of Neoproterozoic mafic rocks and sandstones from northeastern Guizhou, South China: coeval arc magmatism and sedimentation. *Precambrian Research* 170, 27–42.